Transceiver Design and Signal Detection in Backscatter Communication Systems With Multiple-Antenna Tags

Chen Chen, Gongpu Wang, *Member, IEEE*, Hao Guan, Ying-Chang Liang, *Fellow, IEEE*, and Chintha Tellambura, *Fellow, IEEE*

***Abstract*— Ambient backscatter technology utilizes ambient radio frequency (RF) signals to enable battery-free devices (tags and readers) to communicate. Most existing studies assume single-antenna tags. However, in this paper, we consider tags with multiple antennas, which are exploited to provide transmit diversity. Channel state information (CSI) estimation is then a fundamental challenge because the tags can transmit few or no training symbols. To overcome it, we require detectors that operate without CSI. Thus, we propose and design three detectors based on the chi-squared test, F-test and Bartlett's test. The latter two are blind detectors because they require neither CSI nor the knowledge of RF source power and noise variance. We derive the detection probability bounds for the first two detectors. We also propose optimal tag antenna selection schemes to maximize the detection probabilities. Finally, simulation results are provided to corroborate our theoretical studies.**

***Index Terms*— Ambient backscatter, Bartlett's test, chi-squared test, F-test, multiple antennas, probability of detection, signal detection.**

I. Introduction

THE Internet of Things (IoT) [1] has been attracting significant interest in recent years. The basic idea is ubiquitous connectivity among a variety of things in both domestic and work fields. These objects are embedded with small computing devices such as radio frequency identification (RFID) tags, sensors and actuators to perform different functions. The IoT enables these devices to interact and cooperate.

However, the widespread development and deployment of IoT face a key energy challenge: these device batteries, especially of sensors and tags, have limited lifetime and incur maintenance costs. These sensors may also be limited by severe external conditions. For example, it is almost impossible to replace batteries of sensors embedded in walls. Moreover, sensors and their batteries in beach areas suffer from sea water corrosion [2].

An efficient strategy to address this problem is to harvest energy from the ambient environment, instead of utilizing batteries. Ambient sources typically include solar, wind, vibrational and electromagnetic (EM) signals. Solar, wind and vibrational sources are often unstable and subject to the vagaries of the environment; in contrast, ambient EM is a good stable energy source for sensors in IoT [2], [3].

One well-known application of EM energy harvesting is RFID. A typical RFID system contains a reader and a tag. The reader generates a continuous EM wave, and the tag receives and re-modulates it. This process is often referred to as radio backscatter [4], [5], a type of wireless communication exploiting the reflection of EM waves. The basic principle is that the tag responds to the reader by changing its antenna impedance and modulating its own information onto the backscattered wave [6]. Since tags utilize EM energy from the reader and thus do not need to generate radio waves themselves, radio backscatter does away with the tag battery and hence lowers the cost of the tag.

However, a drawback of conventional radio backscatter is that one dedicated power source (a RFID reader) is required to drive the battery-free tag. To overcome this disadvantage, ambient backscatter is proposed in [3], [7], which enables battery-free tags to communicate with other devices through remodulating and backscattering ambient radio frequency (RF) signals, such as existing television (TV) and cellular signals. The fundamental idea of ambient backscatter is that the tag transmits a '1' or '0' bit through switching the antenna impedance which results in reflecting or absorbing states. Clearly, ambient backscatter exploits wireless signals for both energy harvesting and communication and therefore can free tags or sensors from dedicated power sources and batteries.

Manuscript received April 3, 2019; revised September 13, 2019 and January 6, 2020; accepted January 24, 2020. Date of publication February 12, 2020; date of current version May 8, 2020. This work was supported in part by the Key Laboratory of Universal Wireless Communications (BUPT), Ministry of Education, China, under Grant KFKT-2018104, in part by the Natural Science Foundation of China (NSFC) under Grant 61571037, Grant 61871026, and Grant U1834210, and in part by the NFSC Outstanding Youth under Grant 61725101. This article was presented in part at the IEEE APCC 2018. The associate editor coordinating the review of this article and approving it for publication was D. C. Popescu. *(Corresponding author: Gongpu Wang.)*

Chen Chen and Gongpu Wang are with the Beijing Key Laboratory of Transportation Data Analysis and Mining, School of Computer and Information Technology, Beijing Jiaotong University, Beijing 100044, China (e-mail: 16120355@bjtu.edu.cn; gpwang@bjtu.edu.cn).

Hao Guan is with Nokia Bell Labs, Beijing 100102, China (e-mail: hao.guan@nokia-sbell.com).

Ying-Chang Liang is with the Center for Intelligent Networking and Communications, University of Electronic Science and Technology of China, Chengdu 611731, China (e-mail: liangyc@ieee.org).

Chintha Tellambura is with the Department of Electrical and Computer Engineering, University of Alberta, Edmonton, AB T6G 2V4, Canada (e-mail: chintha@ece.ualberta.ca).

Color versions of one or more of the figures in this article are available online at http://ieeexplore.ieee.org.

Digital Object Identifier 10.1109/TWC.2020.2971990

Several ambient backscatter hardware prototypes have been realized. Reference [3] demonstrates the feasibility of ambient backscatter communication by using TV signals for the first time. RF-powered devices [8] connect with the Internet through reflecting existing Wireless Fidelity (Wi-Fi) signals. In [9], multiple-antenna cancelation and coding mechanism are developed to significantly expand the communication range of ambient backscatter systems. Passive Wi-Fi is introduced in [10] to directly generate Wi-Fi transmissions through backscatter and achieves higher data rates than [9].

Theoretical studies of ambient backscatter include channel estimation [11]–[13], signal detection [14]–[20], coding schemes [21], [22], tag selection schemes [23]–[25], and performance analysis such as bit error rate (BER), achievable data rates, and ergodic and outage capacities [26]–[28]. The authors in [14] and [15] design a differential encoding scheme that eliminates the necessity of channel estimation and decodes the tag information via signal power difference. A semi-coherent detector is proposed in [16], where channel-related parameters are estimated from unknown data symbols and a few pilot symbols. Reference [19] converts the signal detection problem to a clustering problem by using the the constellation information of the RF source. Furthermore, [20] proposes a cooperative ambient backscatter communication system to recover the information both from the tag and from the RF source. To overcome channel fading and enlarge the communication range, [17] and [18] exploit multiple-antenna readers, investigate the signal detection problem and analyze the BER performance. Ambient backscatter systems with multiple single-antenna tags are also investigated, including tag selection scheme and the corresponding detector design [23], capacity performance analysis [24], and collision avoidance strategy design [25].

Almost all current ambient backscatter research assumes a single-antenna tag [14]–[28]. In practice, a multiple-antenna tag offers the following benefits:

1) Unlike a single-antenna tag [3], it can enable the simultaneous energy harvesting and backscattering [41], [42].
2) It may enlarge the communication range between the tag and the reader [29].
3) It can yield larger diversity gains compared to signal-antenna tags, which will enhance communication reliability and lower the system BER [30], [31].
4) It can enable the reader to perform signal detection without the knowledge of RF signal power, noise variance and channel state information (CSI).

In this paper, we therefore introduce the use of multiple-antenna tags. Clearly, they open a myriad of research opportunities such as energy harvesting and utilization, encoding and decoding methods, antenna selection at the tag and signal detection at the reader. These opportunities are left as future research topics.

Herein, we focus on detection of the signals from multiple-antenna tags. Existing detectors for single-antenna tag based systems [14]–[18] cannot be extended straightforwardly for multiple-antenna tags for the following reasons:

1) Multiple antennas result in multiple, coexisting wireless channels. Previous works usually assume the availability of perfect knowledge of the RF signal power, noise variance and CSI at the reader. In practice, these parameters may be unknown, especially when using multiple-antenna tags, because few or no training symbols can be transmitted by the tag due to limited power availability with wireless energy harvesting.
2) Due to the inaccessible multiple channel parameters between the tag and the reader, traditional detectors like the Neyman-Pearson (NP) test [32], which is equivalent to energy detection, cannot recover the signals from multiple-antenna tags. The reason is that these detectors fail to find sufficient statistics (see [33] and references therein). Moreover, as proved in our previous work [34], the generalized likelihood ratio test (GLRT) [35], a traditional approach for the signal detection with unknown parameters, requires specially designed backscatter schemes with a quantized number of RF signals per antenna, which may limit its extensive applications in various scenarios.
3) Antenna selection at the tag facilitates energy harvesting and backscattering simultaneously. This option does not exist for the case of single-antenna tags.

A Wi-Fi backscatter communications system with multiple-antenna tags has been proposed in [36]. Each tag is equipped with only two antennas, and each antenna reflects the signals from the Wi-Fi AP using different powers. However, an 8-bit preamble is required to perform tag signal detection, which consumes more energy. Thus, in this paper, we equip the tag with an arbitrary number of antennas and design three ambient-scatter detectors based on the variance test [38]. This allows a much more flexible backscatter scheme. The contributions of this paper are listed as follows:

- We utilize multiple-antenna tags and design the corresponding backscatter schemes to perform energy harvesting and backscatter modulation simultaneously.
- Three ambient-scatter detectors with multiple-antenna tags are proposed based on the chi-squared test, F-test and Bartlett's test, respectively. These require neither CSI nor the RF signal power and the noise variance at the reader.
- The upper and lower bounds on the detection probabilities for the chi-squared based detector and the F-test detector are derived, respectively. We also obtain detection probabilities for several special cases.
- The optimal backscatter antenna selection schemes are proposed to provide the transmit diversity and further maximize the detection performance.

This paper is organized as follows. Section II proposes the theoretical model for ambient backscatter systems with multiple-antenna tags. Section III presents a chi-squared based detector, obtains the upper and lower bounds on its detection probability, and investigates optimal antenna selection. Section IV develops an F-test detector and derives the lower and upper bounds on the detection probability. An optimal antenna selection algorithm is also suggested. Section V designs the Bartlett detector and investigates the tag antenna selection scheme. Simulation results are provided in Section VI and conclusions are drawn in Section VII.

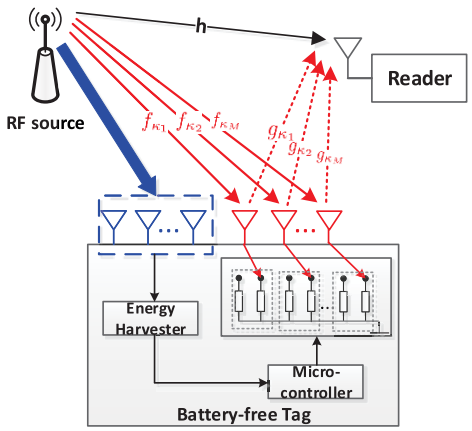

Fig. 1. An ambient backscatter system with a multiple-antenna tag.

Notation: Throughout the paper, scalars, vectors and matrices are denoted by lowercase, boldface lowercase, and boldface uppercase letters, respectively. The absolute value of a scalar y is indicated by $|y|$. For vector $\mathbf{y}$, the Euclidean norm, the transpose, and the Hermitian transpose are denoted by $\|\mathbf{y}\|_2$, $\mathbf{y}^T$ and $\mathbf{y}^H$, respectively. For matrix $\mathbf{Y}$, the Hermitian transpose is given by $\mathbf{Y}^H$. The matrix $\mathbf{I}_N$ represents the $N\times N$ identity matrix. The cardinality of the set $\mathcal{A}$ is $|\mathcal{A}|$ and the ith element of the set is $\mathcal{A}(i)$. We use $\mathcal{CN}(\mu,\sigma^2)$, χ_d^2, and F_{d_1,d_2} to indicate the complex Gaussian distribution with mean μ and variance σ^2, the chi-squared distribution with d degrees of freedom, and the F distribution with d_1 and d_2 degrees of freedom, respectively.

II. System Model

A. System Description

The ambient backscatter communication system (Fig. 1) is composed of an RF source, a single-antenna reader and a tag with K antennas, which are divided into two sets: backscatter antenna set $\mathcal{B}$ with M $(1 \le M \le K)$ antennas and energy harvesting antenna set $\mathcal{E}$ with $K-M$ antennas.

When the RF source broadcasts its signals, both the tag and the reader receive them. To transmit the tag information, the tag selects only one active backscatter antenna from $\mathcal{B}$ each time and adjusts the corresponding load impedance between reflecting and non-reflecting states. The $K-M$ antennas from $\mathcal{E}$ remain the energy harvesting state and collect energy from the RF signals and the signals backscattered by the active backscatter antenna. Besides, the rest $M-1$ silent backscatter antennas from $\mathcal{B}$ can also help with energy harvesting. Therefore, the energy captured by both the $K-1$ antennas provides the power required by the micro-controller and by the active backscatter antenna. Finally, the reader receives the superposition of the RF signals and the backscattered signals.

For simplicity, we indicate the candidate antenna set $\mathcal{A}$ as $\{1,2,\ldots,K\}$ and the backscatter antenna set $\mathcal{B}$ as $\{\kappa_1,\kappa_2,\ldots,\kappa_M\}$. The multiple-antenna tag channels for typical backscatter communication systems have been studied in detail by [29], [30], where each tag antenna is regarded as a pinhole. A pinhole enable the signals from the multiple paths to be superimposed at a single point and the channels corresponding to the multiple antennas are independent [39].

In our system with the multiple-antenna tags, there exist M pinholes, which lead to M independent channels. Denote the channels between the RF source and the reader, between the RF source and the mth backscatter antenna of the tag, and between this antenna and the reader as h, f_{κ_m}, and g_{κ_m}, respectively, where $1 \le m \le M$. Since the ambient source locates far away from both the tag and the reader, compare with the distance between the reader and the tag, we assume that h and f_{κ_m} suffer from the Rayleigh fading, while g_{κ_m} obeys Rician fading. Further, a frequency-flat and block-fading channel model is assumed.

B. The Tag Operation

Similar to the previous works [3], [14]–[16], [20], the key insight of our proposed backscatter scheme is that the tag will transmit at a much lower rate than the rate of the RF source due to the strict power constraint. Assume that the RF source transmits N complex Gaussian random signals $\{x(n), n = 1,\ldots,N\}$ with transmitted power P_s in one time slot, i.e., $\mathbf{x} = [x(1),x(2),\ldots,x(N)]^T$. Moreover, $x(n)$ for $n = 1,\ldots,N$ are independent and identically distributed.

As Fig. 3 shows, the tag signal B remains unchanged during N consecutive $x(n)$, where $B = 0$ indicates that the RF signals are absorbed and $B = 1$ means that the RF signals are reflected. Then, we divide the N RF signals in one time slot into M sets, and each set contains N_m consecutive RF signals, i.e., $\sum_{m=1}^{M} N_m = N$. The mth RF signal set $\mathbf{x}_m$ is given by

$$\begin{aligned}&\mathbf{x}_m\\&= [x_m(1),x_m(2),\ldots,x_m(N_m)]^T\\&= \left[x\left(\sum_{i=1}^{m-1}N_i+1\right),x\left(\sum_{i=1}^{m-1}N_i+2\right),\ldots,x\left(\sum_{i=1}^{m}N_i\right)\right]^T\end{aligned} \tag{1}$$

where $1 \le m \le M$ and $N_0 = 0$.

When the RF source transmits the mth RF signal set, the mth backscatter antenna κ_m is active and reflects the RF signals in the mth set; that is, only one backscatter antenna is selected at one time for backscattering. Mathematically, the signal received at the mth backscatter antenna of the tag $\mathbf{r}_m(n)$ can be expressed as $f_{\kappa_m}\mathbf{x}_m$.

After this reception, the backscattered signal by the mth backscatter antenna is

$$\mathbf{r}_b^m(n) = \alpha B \mathbf{r}_m(n), \tag{2}$$

where α represents the attenuation inside the tag.

The other $K-1$ antennas are all connected to the energy harvester, and collect energy from both the RF signals and the backscattered signals of the mth backscatter antenna.[1] A schematic of energy harvesting is given to clearly show

[1]The amount of harvested energy is typically on the order of micro-watts [41], which is sufficient for powering the analog components of the ambient backscatter devices, which consume a minimum of 0.79 μW [3].

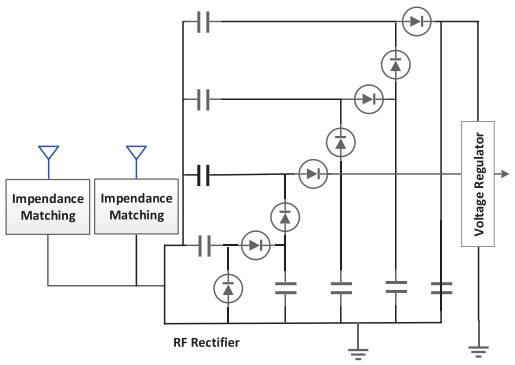

Fig. 2. A schematic of energy harvesting.

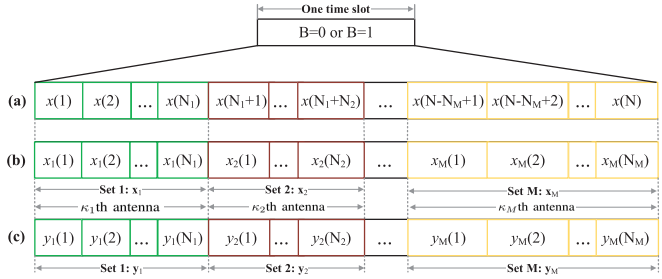

Fig. 3. Backscatter scheme of the tag in one slot: (a) N RF signals received by the tag, (b) backscattered signals by M backscatter antennas, (c) N received signals at the reader.

how to obtain wireless energy from two antennas simultaneously [40]–[42] As Fig. 2 shows, the matching networks provide maximum power transfer from the energy harvesting antennas to the rectifier. Then a 4 stage charge pump converts the incoming power of the multiple energy harvesting antennas to voltage. Finally, the direct current (DC) voltage is stored in a large capacitor and supplied to a regulator to power the micro-controller of the battery-less tag. Due to the nonlinear RF-DC conversion through an rectifier and diode circuit, and the load-independent energy harvesting efficiency, the energy harvester is a non-linear device.[2]

Note that single-antenna tags must perform the transmit and energy harvesting operations one after other [3]. Specifically, when the tag is transmitting information, energy harvesting is not possible, and vice versa. In contrast, our proposed multi-antenna tag scheme avoids this bottleneck. The tag could reflect the RF signals with the selected backscatter antennas and capture energy with the residual $K-1$ antennas simultaneously.

C. The Reader Operation

As Fig. 3 shows, corresponding to the M RF signal sets, the received signals at the tag can be also divided into M sets. Under the assumption of perfect synchronization among the battery-less tag, the RF source, and the reader [3], [27], the received signal at the reader in the mth set is the superposition of the signal from the RF source and the modulated signal backscattered from the mth backscatter antenna of the tag, which is given by

$$\begin{aligned}\mathbf{y}_m &= h\mathbf{x}_m + g_{\kappa_m}\mathbf{r}_b^m(n) + \boldsymbol{\omega}_m \\ &= \begin{cases} h\mathbf{x}_m + \boldsymbol{\omega}_m, & B=0, \\ h\mathbf{x}_m + \alpha f_{\kappa_m} g_{\kappa_m}\mathbf{x}_m + \boldsymbol{\omega}_m, & B=1, \end{cases}\end{aligned} \tag{3}$$

where

$$\mathbf{y}_m = [y_m(1), y_m(2), \ldots, y_m(N_m)]^T, \tag{4}$$

and $\boldsymbol{\omega}_m = [\omega_m(1), \omega_m(2), \ldots, \omega_m(N_m)]^T \sim \mathcal{CN}(\mathbf{0}, \sigma_0^2\mathbf{I}_{N_m})$ is the additive white Gaussian noise (AWGN) at the reader. Define the combined channel that corresponds to the mth backscatter antenna as

$$\mu_{\kappa_m} = h + \alpha f_{\kappa_m} g_{\kappa_m}. \tag{5}$$

In one time slot, the received signals at the reader can be expressed in terms of two hypothesis as

$$\begin{cases} \mathcal{H}_0 : \mathbf{y} = h\mathbf{x} + \boldsymbol{\omega}, & B=0, \\ \mathcal{H}_1 : \mathbf{y} = \mathbf{F}\mathbf{x} + \boldsymbol{\omega}, & B=1, \end{cases} \tag{6}$$

where $\mathbf{y} = [\mathbf{y}_1^T, \mathbf{y}_2^T, \cdots, \mathbf{y}_M^T]^T$, $\boldsymbol{\omega} = [\boldsymbol{\omega}_1^T, \boldsymbol{\omega}_2^T, \cdots, \boldsymbol{\omega}_M^T]^T$ and

$$\mathbf{F} = \mathrm{diag}[\underbrace{\mu_{\kappa_1}, \ldots, \mu_{\kappa_1}}_{N_1}, \underbrace{\mu_{\kappa_2}, \ldots, \mu_{\kappa_2}}_{N_2}, \ldots, \underbrace{\mu_{\kappa_M}, \ldots, \mu_{\kappa_M}}_{N_M}]. \tag{7}$$

The reader aims to recover the tag signal B via the hypothesis testing problem (6) under different assumptions on the knowledge of the RF signal power P_s, the noise variance σ_0^2 and the CSI, i.e., h and μ_{κ_m}.

To end it, we first notice that the received signals $\mathbf{y}$ in (6) are then distributed as

$$\begin{cases} \mathcal{H}_0 : \mathbf{y} \sim \mathcal{CN}(\mathbf{0}, \mathbf{C}_0), & B=0, \\ \mathcal{H}_1 : \mathbf{y} \sim \mathcal{CN}(\mathbf{0}, \mathbf{C}_1), & B=1, \end{cases} \tag{8}$$

where $\mathbf{C}_0$ and $\mathbf{C}_1$ are the covariance matrices under $\mathcal{H}_0$ and $\mathcal{H}_1$, respectively, and can be derived as

$$\begin{aligned}\mathbf{C}_i &= \mathbb{E}\{(\mathbf{y} - \mathbb{E}\{\mathbf{y}\})(\mathbf{y} - \mathbb{E}\{\mathbf{y}\})^H\} \\ &= \begin{cases} (|h|^2 P_s + \sigma_0^2)\mathbf{I}_N, & i=0, \\ \mathbf{F}\mathbf{F}^H P_s + \sigma_0^2\mathbf{I}_N, & i=1. \end{cases}\end{aligned} \tag{9}$$

The covariance matrix $\mathbf{C}_0$ under $\mathcal{H}_0$ is a diagonal matrix with identical diagonal elements $|h|^2P_s + \sigma_0^2$, while the covariance matrix $\mathbf{C}_1$ under $\mathcal{H}_1$ is a diagonal matrix with unequal diagonal elements $|\mu_{\kappa_m}|^2 P_s + \sigma_0^2$ due to multiple combined channels. Thus, the difference between the covariance matrices $\mathbf{C}_0$ and $\mathbf{C}_1$ can be used to decide between null hypothesis $\mathcal{H}_0$ or alternative hypothesis $\mathcal{H}_1$. This can be regarded as a variance test, which will be addressed next.

Remark 1: The variance test depends on the sample variance of the received signals. Since the tag signal B remains unchanged during N consecutive received signals $\{y(n), n = 1, \ldots, N\}$ in one time slot, the adjacent RF signals tend to be more uncorrelated than the adjacent backscatter signals. For this reason, averaging the received signals across one time slot should remove the variations in the ambient RF signals.

[2]Since the energy harvesting antennas and the backscatter antennas operate independently and simultaneously, the energy harvesting model has no effect on the detector design in our work.

III. Chi-Squared Based Detector

As described in Section I, the NP test is not applicable for the case of unknown multiple channel parameters μ_{κ_m}. Therefore, designing a new detector without knowing μ_{κ_m} is practically useful, which is the focus of this section.

To design such a detector, we first notice that the absolute value of the channel parameter from the RF source to the reader $|h|$, the RF signal power P_s and the noise variance σ_0^2 are known at the reader. The modulus value $|h|$ can be derived by following the estimation algorithm given in [11] when the tag is in non-reflecting state. Based on these known parameters, the diagonal element $|h|^2P_s+\sigma_0^2$ of the covariance matrix $\mathbf{C}_0$ under $\mathcal{H}_0$ is treated as a specified value. Then the sample variance of the received signals becomes $\frac{\|\mathbf{y}\|_2^2}{N}$. Due to the difference between the covariance matrices (9), it can be easily found that the ratio of the sample variance to the specified value $\frac{2\|\mathbf{y}\|_2^2}{N(|h|^2P_s+\sigma_0^2)}$ approximates to 1 under $\mathcal{H}_0$, but may be either close to 0 or larger than 1 under $\mathcal{H}_1$. Based on this observation, we propose a new chi-squared based detector that utilizes the two tailed chi-squared test [38] to judge if the sample variance is equal to a specified value $\frac{|h|^2P_s+\sigma_0^2}{2}$ or not.

A. General Case: $K > 1$ and $M > 1$

By utilizing the two tailed chi-squared test, the decision rule of the proposed chi-squared based detector can be expressed as

$$\begin{cases} \text{decide } \mathcal{H}_0, & \text{if } \gamma_l \le \dfrac{2\|\mathbf{y}\|_2^2}{N(|h|^2P_s+\sigma_0^2)} \le \gamma_r, \\ \text{decide } \mathcal{H}_1, & \text{if } \dfrac{2\|\mathbf{y}\|_2^2}{N(|h|^2P_s+\sigma_0^2)} \\ & \quad < \gamma_l \text{ or } \dfrac{2\|\mathbf{y}\|_2^2}{N(|h|^2P_s+\sigma_0^2)} > \gamma_r, \end{cases} \tag{10}$$

where the decision thresholds γ_l and γ_r will be determined from given false alarm probability P_{FA}. For simplicity, we next define $\|\mathbf{y}\|_2^2$ as the decision statistic T_{CD}. The decision rule (10) can be reduced to

$$\begin{cases} \text{decide } \mathcal{H}_0, & \text{if } \gamma_l^{\mathrm{CD}} \le T_{\mathrm{CD}} \le \gamma_r^{\mathrm{CD}}, \\ \text{decide } \mathcal{H}_1, & \text{if } T_{\mathrm{CD}} < \gamma_l^{\mathrm{CD}} \text{ or } T_{\mathrm{CD}} > \gamma_r^{\mathrm{CD}}, \end{cases} \tag{11}$$

where the left threshold γ_l^{CD} and the right threshold γ_r^{CD} can be computed as below.

Define $T_{\mathrm{CD0}} = \mathbf{y}^H \left(\dfrac{\mathbf{C}_0}{2}\right)^{-1} \mathbf{y}$. It can be readily checked from (8) that under $\mathcal{H}_0$

$$T_{\mathrm{CD0}} = \frac{2\|\mathbf{y}\|_2^2}{|h|^2P_s+\sigma_0^2} = \frac{2T_{\mathrm{CD}}}{|h|^2P_s+\sigma_0^2} \sim \chi_{2N}^2. \tag{12}$$

Thus, the false alarm probability $P_{\mathrm{FA}}^{\mathrm{CD}}$ can be calculated as

$$\begin{aligned} P_{\mathrm{FA}}^{\mathrm{CD}} &= \Pr\{T_{\mathrm{CD}} < \gamma_l^{CD}; \mathcal{H}_0\} + \Pr\{T_{\mathrm{CD}} > \gamma_r^{CD}; \mathcal{H}_0\} \\ &= \Pr\Big\{T_{\mathrm{CD0}} < \frac{2\gamma_l^{\mathrm{CD}}}{|h|^2P_s+\sigma_0^2}; \mathcal{H}_0\Big\} \\ &\quad + \Pr\Big\{T_{\mathrm{CD0}} > \frac{2\gamma_r^{\mathrm{CD}}}{|h|^2P_s+\sigma_0^2}; \mathcal{H}_0\Big\} \\ &= 1 - Q_{\chi_{2N}^2}\left(\frac{2\gamma_l^{\mathrm{CD}}}{|h|^2P_s+\sigma_0^2}\right) \\ &\quad + Q_{\chi_{2N}^2}\left(\frac{2\gamma_r^{\mathrm{CD}}}{|h|^2P_s+\sigma_0^2}\right), \end{aligned} \tag{13}$$

where $Q_{\chi_d^2}(x) = \exp\left(-\dfrac{x}{2}\right) \sum\limits_{k=0}^{\frac{d}{2}-1} \dfrac{\left(\frac{x}{2}\right)^k}{k!}$ is the tail probability of the chi-squared distribution of even degrees of freedom d [32]. By setting a target false alarm probability $P_{\mathrm{FA}}^{\mathrm{CD}}$ [35] and assuming $\Pr\{T_{\mathrm{CD}} < \gamma_l^{\mathrm{CD}}; \mathcal{H}_0\} = \dfrac{P_{\mathrm{FA}}^{\mathrm{CD}}}{2}$ and $\Pr\{T_{\mathrm{CD}} > \gamma_r^{\mathrm{CD}}; \mathcal{H}_0\} = \dfrac{P_{\mathrm{FA}}^{\mathrm{CD}}}{2}$, the thresholds $\gamma_l^{\mathrm{CD}}$and γ_r^{CD} can be obtained as

$$\gamma_l^{\mathrm{CD}} = \frac{|h|^2P_s+\sigma_0^2}{2} Q_{\chi_{2N}^2}^{-1}\left(1 - \frac{P_{\mathrm{FA}}^{\mathrm{CD}}}{2}\right), \tag{14}$$

$$\gamma_r^{\mathrm{CD}} = \frac{|h|^2P_s+\sigma_0^2}{2} Q_{\chi_{2N}^2}^{-1}\left(\frac{P_{\mathrm{FA}}^{\mathrm{CD}}}{2}\right). \tag{15}$$

Without loss of generality, let us assume that the combined channel modulus that correspond to $\mathcal{A}$ and $\mathcal{B}$ are ordered at the reader as

$$|\mu_1| \ge |\mu_2| \ge \ldots \ge |\mu_K|, \tag{16}$$

$$|\mu_{\kappa_1}| \ge |\mu_{\kappa_2}| \ge \ldots \ge |\mu_{\kappa_M}|. \tag{17}$$

We further analyze the probability of detection and provide the following theorem.

Theorem 1: The lower bound of detection probability $P_{D,lb}^{\mathrm{CD}}$ for the chi-squared based detector (11) can be expressed as

$$P_{D,lb}^{\mathrm{CD}} = 1 - Q_{\chi_{2N}^2}\left(\eta_{lb}^{\mathrm{CD}}\gamma_l^{\mathrm{CD}}\right) + Q_{\chi_{2N}^2}\left(\eta_{ub}^{\mathrm{CD}}\gamma_r^{\mathrm{CD}}\right), \tag{18}$$

and the upper bound $P_{D,ub}^{\mathrm{CD}}$ is

$$P_{D,ub}^{\mathrm{CD}} = 1 - Q_{\chi_{2N}^2}\left(\eta_{ub}^{\mathrm{CD}}\gamma_l^{\mathrm{CD}}\right) + Q_{\chi_{2N}^2}\left(\eta_{lb}^{\mathrm{CD}}\gamma_r^{\mathrm{CD}}\right), \tag{19}$$

where $\eta_{lb}^{\mathrm{CD}} = \dfrac{2}{|\mu_{\kappa_1}|^2P_s+\sigma_0^2}$ and $\eta_{ub}^{\mathrm{CD}} = \dfrac{2}{|\mu_{\kappa_M}|^2P_s+\sigma_0^2}$.

Proof: See Appendix A. ∎

Remark 2: Since the RF signal power P_s and the noise variance σ_0^2 are stationary, the order of the channel modulus $|\mu_k|$ (16) is equivalent to the size relationship of the variances $|\mu_k|^2P_s+\sigma_0^2$ corresponding to the K antennas, where $1 \le k \le K$. In order to obtain the K variances, the RF signals in one time slot are divided into K sets corresponding to the K antennas. The tag then transmits bit '1' as a training symbol. By computing and sorting the sample variances of the K received signal sets, the reader estimates the size relationship (16) roughly. Finally, the reader selects the backscatter antennas (Section III-C) and ranks them as (17).

To exploit the size relationship between the channel modulus $|h|$ and the channel modulus $|\mu_{\kappa_m}|$ corresponding to the backscatter antenna $\kappa_m (1 \le m \le M)$, we specify the following theorem.

Theorem 2: When the size relationship between $|h|$ and $|\mu_{\kappa_m}|$ is known, there exist three cases: $|h| < |\mu_{\kappa_M}|$, or

$|h| > |\mu_{\kappa_1}|$, or $|\mu_{\kappa_M}| < |h| < |\mu_{\kappa_1}|$. The detection rule (11) can be reformulated as

$$\begin{cases} T_{\mathrm{CD}} \underset{\mathcal{H}_0}{\overset{\mathcal{H}_1}{\gtrless}} \gamma_1^{\mathrm{CD}}, & \text{if } |h| < |\mu_{\kappa_M}|, \\ T_{\mathrm{CD}} \underset{\mathcal{H}_1}{\overset{\mathcal{H}_0}{\gtrless}} \gamma_2^{\mathrm{CD}}, & \text{if } |h| > |\mu_{\kappa_1}|, \\ (11), & \text{if } |\mu_{\kappa_M}| < |h| < |\mu_{\kappa_1}|, \end{cases} \tag{20}$$

where the new thresholds γ_1^{CD} and γ_2^{CD} are expressed as

$$\gamma_1^{\mathrm{CD}} = \frac{|h|^2 P_s + \sigma_0^2}{2} Q_{\chi^2_{2N}}^{-1}\left(P_{\mathrm{FA}}^{\mathrm{CD}}\right), \tag{21}$$

$$\gamma_2^{\mathrm{CD}} = \frac{|h|^2 P_s + \sigma_0^2}{2} Q_{\chi^2_{2N}}^{-1}\left(1 - P_{\mathrm{FA}}^{\mathrm{CD}}\right). \tag{22}$$

Then the lower bounds of detection probability for these three cases can be simplified as

$$P_{D,lb}^{\mathrm{CD}} = \begin{cases} Q_{\chi^2_{2N}}\left(\eta_{ub}^{\mathrm{CD}} \gamma_1^{\mathrm{CD}}\right), & \text{if } |h| < |\mu_{\kappa_M}|, \\ 1 - Q_{\chi^2_{2N}}\left(\eta_{lb}^{\mathrm{CD}} \gamma_2^{\mathrm{CD}}\right), & \text{if } |h| > |\mu_{\kappa_1}|, \\ (18), & \text{if } |\mu_{\kappa_M}| < |h| < |\mu_{\kappa_1}|, \end{cases} \tag{23}$$

and the upper bounds are

$$P_{D,ub}^{\mathrm{CD}} = \begin{cases} Q_{\chi^2_{2N}}\left(\eta_{lb}^{\mathrm{CD}} \gamma_1^{\mathrm{CD}}\right), & \text{if } |h| < |\mu_{\kappa_M}|, \\ 1 - Q_{\chi^2_{2N}}\left(\eta_{ub}^{\mathrm{CD}} \gamma_2^{\mathrm{CD}}\right), & \text{if } |h| > |\mu_{\kappa_1}|, \\ (19), & \text{if } |\mu_{\kappa_M}| < |h| < |\mu_{\kappa_1}|. \end{cases} \tag{24}$$

Proof: See Appendix B. ∎

B. Special Case: $K \geq 1$ and $M = 1$

In the case that only one selected antenna backscatters all RF signals, i.e., $M = 1$, suppose the κth ($1 \leq \kappa \leq K$) antenna is selected. The detection problem (6) can be simplified as the binary hypothesis test problem

$$\begin{cases} \mathcal{H}_0 : \mathbf{y} = h\mathbf{x} + \boldsymbol{\omega}, & B = 0, \\ \mathcal{H}_1 : \mathbf{y} = \mu_\kappa \mathbf{x} + \boldsymbol{\omega}, & B = 1, \end{cases} \tag{25}$$

and the received signals $\mathbf{y}$ follow the distribution (8), where the covariance matrix $\mathbf{C}_1$ under $\mathcal{H}_1$ is reduced to $(|\mu_\kappa|^2 P_s + \sigma_0^2)\mathbf{I}_N$.

The above hypothesis testing problem (25) can be addressed via decision rule (11). The corresponding detection probability is derived in the following.

Corollary 1: The detection probability of the special case $M = 1$ is given as

$$P_D^{\mathrm{CD}} = 1 - Q_{\chi^2_{2N}}\left(\eta_{\mathrm{CD}} \gamma_l^{\mathrm{CD}}\right) + Q_{\chi^2_{2N}}\left(\eta_{\mathrm{CD}} \gamma_r^{\mathrm{CD}}\right), \tag{26}$$

where $\eta_{\mathrm{CD}} = \dfrac{2}{|\mu_\kappa|^2 P_s + \sigma_0^2}$.

Proof: The same as Theorem 1 and the details omitted. In such case $P_{D,lb}^{\mathrm{CD}} = P_D^{\mathrm{CD}} = P_{D,ub}^{\mathrm{CD}}$. ∎

It is worth noting that selecting only one antenna ($K > 1$ and $M = 1$) leads to the maximal detection probability for the chi-squared based detector, as will be shown in Section III-C.

Corollary 2: For known size relationship between $|h|$ and $|\mu_\kappa|$, the detection probability for the special case can be simplified as

$$P_D^{\mathrm{CD}} = \begin{cases} Q_{\chi^2_{2N}}\left(\eta_{\mathrm{CD}} \gamma_1^{\mathrm{CD}}\right), & \text{if } |\mu_\kappa| \leq |h|, \\ 1 - Q_{\chi^2_{2N}}\left(\eta_{\mathrm{CD}} \gamma_2^{\mathrm{CD}}\right), & \text{if } |\mu_\kappa| > |h|. \end{cases} \tag{27}$$

Proof: The same as proof of Theorem 2. We obtain that $P_{D,lb}^{\mathrm{CD}} = P_D^{\mathrm{CD}} = P_{D,ub}^{\mathrm{CD}}$ for the cases of $|\mu_\kappa| > |h|$ and $|\mu_\kappa| < |h|$, respectively. ∎

Remark 3: Our chi-squared based detector (11) can apply to the cases of both single-antenna tag and multiple-antenna tag. While the existing detectors [14]–[16] only focus on the single-antenna case. Besides, the chi-squared based detector (11) also has the advantage that it can perform detection without any special coding [14], [15], or the information about the size relationship between $|h|$ and $|\mu_{\kappa_m}|$ [16].

C. Optimal Antenna Selection

This subsection investigates the optimal antenna selection scheme that can maximize the detection probability at the reader.

Since the principle of our chi-squared based detector is to compare the sample variance $\dfrac{\|\mathbf{y}\|_2^2}{N}$ with a specified value $|h|^2 P_s + \sigma_0^2$, which can be thought of as the variance of the received signals under $\mathcal{H}_0$. Thus, as proved in [45], to maximize the detection probability, we aim to find the optimal backscatter antenna set $\mathcal{B}_{opt}$ that can maximize the variance difference, i.e., the difference between the average powers of the received signals under $\mathcal{H}_0$ and $\mathcal{H}_1$, which is defined as

$$\delta_E = \left| \mathbb{E}_{\mathbf{x},\omega}\{\|\mathbf{y}\|_2^2; \mathcal{H}_1\} - \mathbb{E}_{\mathbf{x},\omega}\{\|\mathbf{y}\|_2^2; \mathcal{H}_0\} \right|. \tag{28}$$

Proposition 1: The optimal backscatter antenna set that can maximize the energy difference (28) is

$$\begin{aligned} \mathcal{B}_{opt} &= \arg\max_{\mathcal{B} \in \mathcal{A}} \delta_E \\ &= \begin{cases} \mathcal{B}_1, & \text{if } |\mu_K| > |h|, \\ \mathcal{B}_2, & \text{if } |\mu_1| < |h|, \\ \arg\max\limits_{\mathcal{B} \in \{\mathcal{B}_1, \mathcal{B}_2\}} \delta_E, & \text{if } |\mu_1| < |h| < |\mu_K|, \end{cases} \end{aligned} \tag{29}$$

where

$$\mathcal{B}_1 = \{1, 2, \ldots, M\}, \tag{30}$$

$$\mathcal{B}_2 = \{K - M + 1, K - M + 2, \ldots, K - 1, K\}. \tag{31}$$

Proof: See Appendix C ∎

Corollary 3: Selecting only one antenna ($M = 1$) at the tag provides the maximum detection probability at the reader.

Proof: See Appendix D. ∎

IV. F-Test Detector

The existing detectors [14]–[16] and our proposed chi-squared based detector require the knowledge of the channel h, the RF signal power P_s and the noise variance σ_0^2, which in some practical cases may be not available at the

reader because the RF sources (e.g., signal power and location) are uncontrollable and thus the RF signals and the noise are unknown a priori to the reader. For this reason, blind detection without P_s, σ_0^2, and all CSI including both h and μ_k, is preferable for the reader in many applications of ambient backscatter. As shown in [34], the common approaches for the hypothesis testing problem in the presence of unknown parameters, GLRT, needs a specially designed backscatter scheme. Therefore, we need to design a new blind detector that is suitable for wider applications.

To design such a detector, we notice that the received signals at the reader are partitioned into M sets (4) and the variances of the received signals in different sets are equal under $\mathcal{H}_0$ while are probably various under $\mathcal{H}_1$. Hence, if we reorganize the M sets into two groups, the variance ratio of these two group is equal to 1 under $\mathcal{H}_0$, while may far overweight 1 or approximate 0 under $\mathcal{H}_1$. The observation motivates F-test [38], which tests if the variances of two population are equal, and is referred to as F-test detector in this paper. Our F-test detector first computes the sample variances of received signals, then compares the ratios of the variances, and finally decides whether we should accept $\mathcal{H}_0$ or reject it, where the information about RF signals and noise are not required. The detailed steps of our F-test detector are given as below.

A. General Case: $K > 2$ and $M > 2$

We choose an integer number $\tilde{m} \in [1, M-1]$, and reorganize the M sets of the received signals $\mathbf{y}_m$ (4) into two groups:

$$\mathbf{y}_u = [\mathbf{y}_1^T, \mathbf{y}_2^T, \ldots, \mathbf{y}_{\tilde{m}}^T]^T, \tag{32}$$

and

$$\mathbf{y}_d = [\mathbf{y}_{\tilde{m}+1}^T, \mathbf{y}_{\tilde{m}+2}^T, \ldots, \mathbf{y}_M^T]^T. \tag{33}$$

The lengths of $\mathbf{y}_u$ and $\mathbf{y}_d$ are $N_u = \sum_{m=1}^{\tilde{m}} N_m$ and $N_d = \sum_{m=\tilde{m}+1}^{M} N_m$, respectively.

It can be readily checked that

$$\mathcal{H}_0 : \begin{cases} \mathbf{y}_u = h\mathbf{x}_u + \boldsymbol{\omega}_u, \\ \mathbf{y}_d = h\mathbf{x}_d + \boldsymbol{\omega}_d, \end{cases} \tag{34}$$

and

$$\mathcal{H}_1 : \begin{cases} \mathbf{y}_u = \mathbf{F}_u\mathbf{x}_u + \boldsymbol{\omega}_u, \\ \mathbf{y}_d = \mathbf{F}_d\mathbf{x}_d + \boldsymbol{\omega}_d, \end{cases} \tag{35}$$

where $\mathbf{x}_u = [x(1), x(2), \cdots, x(N_u)]^T$, $\mathbf{x}_d = [x(N_u+1), \cdots, x(N-1), x(N)]^T$, and

$$\mathbf{F}_u = \mathrm{diag}[\underbrace{\mu_{\kappa_1}, \ldots, \mu_{\kappa_1}}_{N_1}, \underbrace{\mu_{\kappa_2}, \ldots, \mu_{\kappa_2}}_{N_2}, \ldots, \underbrace{\mu_{\kappa_{\tilde{m}}}, \ldots, \mu_{\kappa_{\tilde{m}}}}_{N_{\tilde{m}}}],$$

$$\mathbf{F}_d = \mathrm{diag}[\underbrace{\mu_{\kappa_{\tilde{m}+1}}, \ldots, \mu_{\kappa_{\tilde{m}+1}}}_{N_{\tilde{m}+1}}, \ldots, \underbrace{\mu_{\kappa_M}, \ldots, \mu_{\kappa_M}}_{N_M}].$$

The first part $\mathbf{y}_u$ has the distribution

$$\mathbf{y}_u \sim \begin{cases} \mathcal{H}_0 : \mathcal{CN}(\mathbf{0}, \mathbf{C}_{u0}), & B = 0, \\ \mathcal{H}_1 : \mathcal{CN}(\mathbf{0}, \mathbf{C}_{u1}), & B = 1, \end{cases} \tag{36}$$

and the second part $\mathbf{y}_d$ has the distribution

$$\mathbf{y}_d \sim \begin{cases} \mathcal{H}_0 : \mathcal{CN}(\mathbf{0}, \mathbf{C}_{d0}), & B = 0, \\ \mathcal{H}_1 : \mathcal{CN}(\mathbf{0}, \mathbf{C}_{d1}), & B = 1, \end{cases} \tag{37}$$

where $\mathbf{C}_{u0} = (|h|^2P_s + \sigma_0^2)\mathbf{I}_{N_u}$, $\mathbf{C}_{u1} = \mathbf{F}_u\mathbf{F}_u^H P_s + \sigma_0^2\mathbf{I}_{N_u}$, $\mathbf{C}_{d0} = (|h|^2P_s + \sigma_0^2)\mathbf{I}_{N_d}$ and $\mathbf{C}_{d1} = \mathbf{F}_d\mathbf{F}_d^H P_s + \sigma_0^2\mathbf{I}_{N_d}$.

We subsequently compute the sample variances of received signals $\mathbf{y}_u$ and $\mathbf{y}_d$ as $\frac{\|\mathbf{y}_u\|_2^2}{N_u}$ and $\frac{\|\mathbf{y}_d\|_2^2}{N_d}$, respectively. When the CSI $\mu_{\kappa_m}, m = 1, 2, \ldots, M$ are unknown, the ratio of sample variances $\frac{N_d\|\mathbf{y}_u\|_2^2}{N_u\|\mathbf{y}_d\|_2^2}$ is expected to approximate to 1 under $\mathcal{H}_0$ while may approximate to 0 or be hopefully larger than 1 under $\mathcal{H}_1$. Based on this fact, we introduce two tailed F test to carry out the binary hypothesis test problem (6)

$$\begin{cases} \text{decide } \mathcal{H}_0, & \text{if } \gamma_l \le \dfrac{N_d\|\mathbf{y}_u\|_2^2}{N_u\|\mathbf{y}_d\|_2^2} \le \gamma_r, \\ \text{decide } \mathcal{H}_1, & \text{if } \dfrac{N_d\|\mathbf{y}_u\|_2^2}{N_u\|\mathbf{y}_d\|_2^2} < \gamma_l \text{ or } \dfrac{N_d\|\mathbf{y}_u\|_2^2}{N_u\|\mathbf{y}_d\|_2^2} > \gamma_r, \end{cases} \tag{38}$$

where γ_l and γ_r are the detection thresholds calculated from given false alarm probability P_{FA} For simplicity, we define the decision statistic for the proposed F-test detector as $T_{\mathrm{FD}} = \frac{\|\mathbf{y}_u\|_2^2}{\|\mathbf{y}_d\|_2^2}$. Then the decision rule (38) can be simplified as

$$\begin{cases} \text{decide } \mathcal{H}_0, & \text{if } \gamma_l^{\mathrm{FD}} \le T_{\mathrm{FD}} \le \gamma_r^{\mathrm{FD}}, \\ \text{decide } \mathcal{H}_1, & \text{if } T_{\mathrm{FD}} < \gamma_l^{\mathrm{FD}} \text{ or } T_{\mathrm{FD}} > \gamma_r^{\mathrm{FD}}. \end{cases} \tag{39}$$

The derivation of the thresholds is given as below.

From (36), we have

$$\begin{cases} \mathcal{H}_0 : \mathbf{y}_u^H \left(\dfrac{\mathbf{C}_{u0}}{2}\right)^{-1} \mathbf{y}_u = \dfrac{2\|\mathbf{y}_u\|_2^2}{|h|^2P_s + \sigma_0^2} \sim \chi_{2N_u}^2, \\ \mathcal{H}_1 : \mathbf{y}_u^H \left(\dfrac{\mathbf{C}_{u1}}{2}\right)^{-1} \mathbf{y}_u = \displaystyle\sum_{m=1}^{\tilde{m}} \dfrac{2\|\mathbf{y}_m\|_2^2}{|\mu_{\kappa_m}|^2P_s + \sigma_0^2} \sim \chi_{2N_u}^2. \end{cases} \tag{40}$$

Similarly, from (37) we obtain

$$\begin{cases} \mathcal{H}_0 : \mathbf{y}_d^H \left(\dfrac{\mathbf{C}_{d0}}{2}\right)^{-1} \mathbf{y}_d = \dfrac{2\|\mathbf{y}_d\|_2^2}{|h|^2P_s + \sigma_0^2} \sim \chi_{2N_d}^2, \\ \mathcal{H}_1 : \mathbf{y}_d^H \left(\dfrac{\mathbf{C}_{d1}}{2}\right)^{-1} \mathbf{y}_d = \displaystyle\sum_{m=\tilde{m}+1}^{M} \dfrac{2\|\mathbf{y}_m\|_2^2}{|\mu_{\kappa_m}|^2P_s + \sigma_0^2} \sim \chi_{2N_d}^2. \end{cases} \tag{41}$$

It can be straightforward derived that under $\mathcal{H}_0$

$$T_{\mathrm{FD0}} = \frac{\dfrac{2\mathbf{y}_u^T\mathbf{C}_{u0}^{-1}\mathbf{y}_u}{2N_u}}{\dfrac{2\mathbf{y}_d^T\mathbf{C}_{d0}^{-1}\mathbf{y}_d}{2N_d}} = \frac{N_d\|\mathbf{y}_u\|_2^2}{N_u\|\mathbf{y}_d\|_2^2} \sim F_{(2N_u, 2N_d)}, \tag{42}$$

and under $\mathcal{H}_1$

$$T_{\mathrm{FD1}} = \frac{\dfrac{2\mathbf{y}_u^H\mathbf{C}_{u1}^{-1}\mathbf{y}_u}{2N_u}}{\dfrac{2\mathbf{y}_d^H\mathbf{C}_{d1}^{-1}\mathbf{y}_d}{2N_d}} = \frac{N_d\mathbf{y}_u^H\mathbf{C}_{u1}^{-1}\mathbf{y}_u}{N_u\mathbf{y}_d^H\mathbf{C}_{d1}^{-1}\mathbf{y}_d} \sim F_{(2N_u, 2N_d)}. \tag{43}$$

According to (39), the false alarm probability $P_{\mathrm{FA}}^{\mathrm{FD}}$ can be obtained as

$$\begin{aligned}P_{\mathrm{FA}}^{\mathrm{FD}} &= \Pr\{T_{\mathrm{FD}} < \gamma_l^{\mathrm{FD}}; \mathcal{H}_0\} + \Pr\{T_{\mathrm{FD}} > \gamma_r^{\mathrm{FD}}; \mathcal{H}_0\} \\ &= \Pr\Big\{T_{\mathrm{FD0}} < \frac{N_d}{N_u}\gamma_l^{\mathrm{FD}}; \mathcal{H}_0\Big\} \\ &\quad + \Pr\Big\{T_{\mathrm{FD0}} > \frac{N_d}{N_u}\gamma_r^{\mathrm{FD}}; \mathcal{H}_0\Big\} \\ &= \int_{\infty}^{\frac{N_d}{N_u}\gamma_l^{\mathrm{FD}}} p(T_{\mathrm{FD0}}; \mathcal{H}_0)\mathrm{d}T_{\mathrm{FD0}} \\ &\quad + \int_{\frac{N_d}{N_u}\gamma_r^{\mathrm{FD}}}^{\infty} p(T_{\mathrm{FD0}}; \mathcal{H}_0)\mathrm{d}T_{\mathrm{FD0}} \\ &= 1 - Q_{F(2N_u,2N_d)}\left(\frac{N_d}{N_u}\gamma_l^{\mathrm{FD}}\right) \\ &\quad + Q_{F(2N_u,2N_d)}\left(\frac{N_d}{N_u}\gamma_r^{\mathrm{FD}}\right), \end{aligned} \tag{44}$$

where $Q_{F(d_1,d_2)}(x) = 1 - \frac{B\left(\frac{d_1 x}{d_1 x + d_2}; \frac{d_1}{2}, \frac{d_2}{2}\right)}{B\left(1; \frac{d_1}{2}, \frac{d_2}{2}\right)}$ represents the tail probability of the F-distribution with parameters d_1 and d_2 at point x [44] and $B(x; a, b) = \int_0^x t^{a-1}(1-t)^{b-1}\mathrm{d}t$ is the incomplete Beta function. By setting a target false alarm probability $P_{\mathrm{FA}}^{\mathrm{FD}}$ and assuming $\Pr\{T_{\mathrm{FD}} < \gamma_l^{\mathrm{FD}}; \mathcal{H}_0\} = \frac{P_{\mathrm{FA}}^{\mathrm{FD}}}{2}$ and $\Pr\{T_{\mathrm{FD}} > \gamma_r^{\mathrm{FD}}; \mathcal{H}_0\} = \frac{P_{\mathrm{FA}}^{\mathrm{FD}}}{2}$, the decision thresholds γ_l^{FD} and γ_r^{FD} for the F-test detector can be directly produced as

$$\gamma_l^{\mathrm{FD}} = \frac{N_u}{N_d} Q^{-1}_{F(2N_u,2N_d)}\left(1 - \frac{P_{\mathrm{FA}}^{\mathrm{FD}}}{2}\right), \tag{45}$$

$$\gamma_r^{\mathrm{FD}} = \frac{N_u}{N_d} Q^{-1}_{F(2N_u,2N_d)}\left(\frac{P_{\mathrm{FA}}^{\mathrm{FD}}}{2}\right). \tag{46}$$

Following the decision rule (39) and utilizing the thresholds (45), we derive the bounds of detection probability.

Theorem 3: Under the assumption (17), the bounds of the detection probability for F-test detector are given by

$$P_{D,lb}^{\mathrm{FD}} = 1 - Q_{F(2N_u,2N_d)}(\eta_{lb}^{\mathrm{FD}}\gamma_l^{\mathrm{FD}}) + Q_{F(2N_u,2N_d)}(\eta_{ub}^{\mathrm{FD}}\gamma_r^{\mathrm{FD}}),$$

and

$$P_{D,ub}^{\mathrm{FD}} = 1 - Q_{F(2N_u,2N_d)}(\eta_{ub}^{\mathrm{FD}}\gamma_l^{\mathrm{FD}}) + Q_{F(2N_u,2N_d)}(\eta_{lb}^{\mathrm{FD}}\gamma_r^{\mathrm{FD}}),$$

where $\eta_{ub}^{\mathrm{FD}} = \frac{N_d(|\mu_{\kappa_{\tilde{m}+1}}|^2 P_s + \sigma_0^2)}{N_u(|\mu_{\kappa_{\tilde{m}}}|^2 P_s + \sigma_0^2)}$ and $\eta_{lb}^{\mathrm{FD}} = \frac{N_d(|\mu_{\kappa_M}|^2 P_s + \sigma_0^2)}{N_u(|\mu_{\kappa_1}|^2 P_s + \sigma_0^2)}$.

Proof: See Appendix E. ∎

When the size relationship of $\mu_{\kappa_m}, m = 1, 2, \ldots, M$ (17) are known at the reader, the proposed F-test detector can be further simplified as follows.

Theorem 4: Given the order of $\mu_{\kappa_m}, m = 1, 2, \ldots, M$ (17), the decision rule (39) is translated into

$$T_{\mathrm{FD}} \underset{\mathcal{H}_0}{\overset{\mathcal{H}_1}{\gtrless}} \gamma_{\mathrm{FD}}, \tag{47}$$

where the threshold γ_{FD} can be expressed as

$$\gamma_{\mathrm{FD}} = \frac{N_u}{N_d} Q^{-1}_{F(2N_u,2N_d)}\left(P_{\mathrm{FA}}^{\mathrm{FD}}\right). \tag{48}$$

Then the detection probability of the F-test detector is bounded as

$$P_{D,lb}^{\mathrm{FD}} = Q_{F(2N_u,2N_d)}(\eta_{ub}^{\mathrm{FD}}\gamma_{\mathrm{FD}}), \tag{49}$$

$$P_{D,ub}^{\mathrm{FD}} = Q_{F(2N_u,2N_d)}(\eta_{lb}^{\mathrm{FD}}\gamma_{\mathrm{FD}}). \tag{50}$$

Proof: See Appendix F. ∎

B. Special Case: $K > 1$ and $M = 2$ (Choosing Two Antennas)

In the case of two antennas are selected to transmit the tag signals, we denote the backscatter antenna set as $\mathcal{B} = \{\kappa_1, \kappa_2\}$, and the corresponding combined channels as μ_{κ_1} and μ_{κ_2}. Likewise, our F-test detector first partitions the N received signals $\mathbf{y}$ into two sets $\mathbf{y}_u = [y_1(1), y_1(2), \ldots, y_1(N_1)]^T$ and $\mathbf{y}_d = [y_2(1), y_2(2), \ldots, y_2(N_2)]^T$, where $N = N_1 + N_2$. Then, we detect the tag signals by using the decision rule (39). Finally, the semi-closed-form detection probability can be derived as follows.

Corollary 4: When the CSI μ_{κ_m} is unknown at the reader, the detection probability of our F-test detector in the case of $M = 2$ can be expressed as

$$\begin{aligned}P_D^{\mathrm{FD}} &= 1 - Q_{F(2N_1,2N_2)}\left(\eta_{\mathrm{FD}}\gamma_l^{\mathrm{FD}}\right) \\ &\quad + Q_{F(2N_1,2N_2)}\left(\eta_{\mathrm{FD}}\gamma_r^{\mathrm{FD}}\right). \end{aligned} \tag{51}$$

Proof: Following the steps similar in Theorem 3, we obtain the detection probability $P_{D,lb}^{\mathrm{FD}} = P_D^{\mathrm{FD}} = P_{D,ub}^{\mathrm{FD}}$. ∎

Corollary 5: When the CSI μ_{κ_m} is known at the reader, the detection probability of our F-test detector in the case of $M = 2$ can be expressed as

$$P_D^{\mathrm{FD}} = Q_{F(2N_1,2N_2)}(\eta_{\mathrm{FD}}\gamma_{\mathrm{FD}}). \tag{52}$$

Proof: Similar as the proof of Theorem 4, we can have $P_{D,lb}^{\mathrm{FD}} = P_D^{\mathrm{FD}} = P_{D,ub}^{\mathrm{FD}}$. ∎

C. Optimal Antenna Selection

Since the principle of our F-test detector is to compare the variance of two groups $\mathbf{y}_u$ and $\mathbf{y}_d$. Thus, as proved in [45], to maximize the detection probability, we aim to find the optimal backscatter antenna set $\mathcal{B} = \{\kappa_1, \kappa_2, \ldots, \kappa_M\}$ that can maximize the variance difference between $\mathbf{y}_u$ and $\mathbf{y}_d$ under $\mathcal{H}_1$, i.e., the difference between the average powers of the signals $\mathbf{y}_u$ and $\mathbf{y}_d$, that is,

$$\max \frac{\sigma_u^2}{\sigma_d^2} \Leftrightarrow \max \frac{\mathbb{E}_{\mathbf{x}_u,\omega_u}\{\|\mathbf{y}_u\|_2^2\}}{\mathbb{E}_{\mathbf{x}_d,\omega_d}\{\|\mathbf{y}_d\|_2^2\}} = \frac{\max \mathbb{E}_{\mathbf{x}_u,\omega_u}\{\|\mathbf{y}_u\|_2^2\}}{\min \mathbb{E}_{\mathbf{x}_d,\omega_d}\{\|\mathbf{y}_d\|_2^2\}}. \tag{53}$$

It can be easily found that

$$\begin{aligned}\mathbb{E}_{\mathbf{x}_u,\omega_u}\{\|\mathbf{y}_u\|_2^2\} &= \mathbb{E}_{\mathbf{x}_u}\{\mathbf{x}_u^H \mathbf{F}_u^H \mathbf{F}_u \mathbf{x}_u\} + \sum_{m=1}^{\tilde{m}} N_m \sigma_0^2 \\ &= P_s \mathrm{trace}(\mathbf{F}_u \mathbf{F}_u^H) + \sum_{m=1}^{\tilde{m}} N_m \sigma_0^2 \\ &= \sum_{m=1}^{\tilde{m}} N_m \left(|\mu_{\kappa_m}|^2 P_s + \sigma_0^2\right). \end{aligned} \tag{54}$$

Therefore, to maximize $\mathbb{E}_{\mathbf{x}_u,\omega_u}\{\|\mathbf{y}_u\|_2^2\}$, those $\tilde{m}$ antennas corresponding to $|\mu_1|, |\mu_2|, ..., |\mu_{\tilde{m}}|$ in (16), i.e., with the first $\tilde{m}$ largest channel gains, should be selected.

Similarly, we can obtain

$$\mathbb{E}_{\mathbf{x}_d,\omega_d}\{\|\mathbf{y}_d\|_2^2\} = \sum_{m=\tilde{m}+1}^{M} N_m \left(|\mu_{\kappa_m}|^2 P_s + \sigma_0^2\right). \quad (55)$$

Hence, in order to minimize $\mathbb{E}_{\mathbf{x}_d,\omega_d}\{\|\mathbf{y}_d\|_2^2\}$, we should select the antennas with the last $(M-\tilde{m})$ smallest channel gains to backscatter $\mathbf{x}_d$.

We summarize the optimal antenna selection mechanism in Algorithm 1. After antenna selection, the selected tags will backscatter the signals to the reader, and then the reader divides the received signals into two parts $\mathbf{y}_u$ and $\mathbf{y}_d$. The optimal boundary $\tilde{m}$ can be computed as

$$\tilde{m} = \underset{1\le m\le M-1}{\arg\min} \{\mu_{\kappa_m} \big| |\mu_{\kappa_1}| - |\mu_{\kappa_m}| < |\mu_{\kappa_m}| - |\mu_{\kappa_M}|\}. \quad (56)$$

Corollary 6: Among all possible antenna selection sets, i.e., $\forall M \in [2, K]$, the set of $\mathcal{B} = \{1, K\}$ $(M = 2)$ provides the largest variance difference, which leads to the highest detection probability for our F-test detector.

Algorithm 1 Selecting the Optimal Backscatter Antennas

Input: The number of selected antennas M; the candidate antenna set $\mathcal{A} = \{1, 2, \ldots, K\}$; the size relationship (16)

Output: The optimal backscatter antenna set $\mathcal{B}_{opt} = \{\kappa_1, \kappa_2, \ldots, \kappa_M\}$

$\kappa_1 = 1$; $\kappa_M = K$; $\mathcal{A}- = \mathcal{A}(1)$; $\mathcal{A}- = \mathcal{A}(K)$;
for $2 \le m \le M-1$ **do**
  $L = |\mathcal{A}|$; $i = \mathcal{A}(1)$; $j = \mathcal{A}(L)$
  if $|\mu_{\kappa_1}|-|\mu_i| < |\mu_j|-|\mu_{\kappa_M}|$ **then** $\kappa_m = i$; $\mathcal{A}- = \mathcal{A}(1)$;
  else $\kappa_m = j$; $\mathcal{A}- = \mathcal{A}(L)$;
  end if
end for
return The optimal backscatter antenna set $\mathcal{B}_{opt}$

Proof: See Appendix G. ∎

V. Bartlett Based Detector

In this section, another blind detector, called Bartlett based detector, is proposed to recover the tag signals without any requirement on P_s, σ_0^2, h, and μ_k.

A. Detector Design

Denote the variances of the received signals $\mathbf{y}_m$ (4) as σ_m^2. We can find that $\sigma_1^2 = \sigma_2^2 = \ldots = \sigma_M^2 = |h|^2 P_s + \sigma_0^2$ under $\mathcal{H}_0$, while $\sigma_m^2 = |\mu_{\kappa_m}|^2 P_s + \sigma_0^2$ under $\mathcal{H}_1$, which indicates that various antenna selection will result in different variances σ_m^2 under $\mathcal{H}_1$. As a result, the hypothesis testing problem (6) can be redefined as

$$\begin{cases} \mathcal{H}_0 : \sigma_i^2 = \sigma_j^2, & B = 0, \\ \mathcal{H}_1 : \sigma_i^2 \ne \sigma_j^2, & B = 1, \end{cases} \quad (57)$$

where $i, j = 1, 2, \ldots, M$ and $i \ne j$.

Our Bartlett based detector,[3] first obtains the maximum likelihood estimate (MLE) of variances of each set $\mathbf{y}_m$, then computes the pooled variance[4] and finally forms a statistic which has the chi-squared distribution. The detailed steps are presented as below.

The MLE of the variances of each set $\mathbf{y}_m$ can be derived as follows. Note that the PDF of $\mathbf{y}_m$ is given by

$$p(\mathbf{y}_m) = \frac{1}{(\pi\sigma_m^2)^{N_m}} \exp\left(-\frac{\|\mathbf{y}_m\|_2^2}{\sigma_m^2}\right). \quad (58)$$

Clearly, the likelihood function of the received signals $\mathbf{y}$ can be expressed as

$$\begin{aligned} L(\mathbf{y}; \sigma_m^2) &= \prod_{m=1}^{M} p(\mathbf{y}_m) \\ &= \frac{1}{\pi^N \Pi_{m=1}^{M} (\sigma_m^2)^{N_m}} \exp\left(-\sum_{m=1}^{M} \frac{\|\mathbf{y}_m\|_2^2}{\sigma_m^2}\right). \end{aligned}$$

By computing $\dfrac{\partial \ln L(\mathbf{y}; \sigma_m^2)}{\partial \sigma_m^2} = 0$, we obtain the MLE of σ_m^2 as

$$\hat{\sigma}_m^2 = \frac{1}{N_m}\|\mathbf{y}_m\|_2^2, m = 1, 2, \ldots, M. \quad (59)$$

Next, the pooled variance can be computed as [46]

$$\sigma_p^2 = \frac{1}{N}\sum_{m=1}^{M} N_m \hat{\sigma}_m^2. \quad (60)$$

Finally, the MLE of variances of each set (59), the pooled variance (60) and the length of each set $N_m, m = 1, 2, \ldots, M$ yield the decision statistic

$$T_{\mathrm{BD}} = \frac{N \ln \sigma_p^2 - \sum_{m=1}^{M} (N_m - 1) \ln\left(\dfrac{N_m}{N_m - 1}\hat{\sigma}_m^2\right)}{1 + \dfrac{1}{3(M-1)}\left(\sum_{m=1}^{M} \dfrac{1}{N_m - 1} - \dfrac{1}{N}\right)}. \quad (61)$$

According to the definition of Bartlett's test [38], if $N_m \ge 5, m = 1, 2, \ldots, M$, the test statistic (61) is a chi-squared random variable (RV) with $M-1$ degrees of freedom. Thus the detection rule of our Bartlett based detector is given by

$$T_{\mathrm{BD}} \underset{\mathcal{H}_0}{\overset{\mathcal{H}_1}{\gtrless}} \gamma_{\mathrm{BD}}, \quad (62)$$

where $\gamma_{\mathrm{BD}} = Q^{-1}_{\chi^2_{M-1}}(P_{\mathrm{FA}}^{\mathrm{BD}})$ is found from a target false alarm probability $P_{\mathrm{FA}}^{\mathrm{BD}}$.

B. Optimal Antenna Selection

Here, we investigate the problem of optimal antenna selection of the Bartlett detector to maximize the variance difference among received signals in M sets.

[3] Bartlett's test is to find if multiple populations have equal variances [38]

[4] Pooled variance is a weighted average of the variances for multiple populations [46].

When $M = 2$, i.e., the backscatter antenna set is given by $\mathcal{B} = \{\kappa_1, \kappa_2\}$, the maximal difference between the variances of $\mathbf{y}_1$ and $\mathbf{y}_2$ is derived as

$$\max_{\kappa_1,\kappa_2\in\{1,2,\ldots,K\}} |\sigma_1^2 - \sigma_2^2| = \max_{\kappa_1,\kappa_2\in\{1,2,\ldots,K\}} \big||\mu_{\kappa_1}|^2 - |\mu_{\kappa_2}|^2\big| P_s. \quad (63)$$

Given the assumption (17), the optimal backscatter antenna set is $\mathcal{B} = \{1, K\}$, i.e., $\mu_{\kappa_1} = \mu_1$ and $\mu_{\kappa_2} = \mu_K$.

When $M > 2$, we first reorganize the received signals $\mathbf{y}$ into two sets and then investigate the variance difference between the two sets. By computing and comparing the average energy of the two set as (54) and (55), the optimal antenna selection scheme for the Bartlett detector is the same as that for F-test detector in Algorithm 1.

Remark 4: The detection probabilities of the Bartlett detector and the F-test detector are raised with larger N_1 and N_M. However, enlarging N_1 can enhance detection probability for the chi-squared based detector only when the backscatter antenna set is $\mathcal{B}_1$ (30). When the backscatter antenna set is $\mathcal{B}_2$ (31), the chi-squared based detector should enlarge N_M, instead of N_1, to improve its detection probability.

Remark 5: The reader performs optimal backscatter antenna selection for the three proposed detectors, and it requires KN complex multipliers and adders (CMAs), and one comparator [34]. While the tag only receives the selection results and activates the corresponding antennas. Thus, the tag complexity is modest and needs an envelope detector and an averaging analog circuit only.

VI. Simulation Results

In this section, we numerically examine the detection performances of the chi-squared based detector (CD), F-test detector (FD) and Bartlett based detector (BD). In normal settings, the distances from the RF source to the tag and reader are large, and that from the tag to the reader is short. The channels in the former case are Rayleigh, and the channels in the latter case are Rician. Therefore, we generate the channel coefficient between the RF source and the reader h and those between the RF source and the tag f_k $(1 \le k \le K)$ according to $\mathcal{CN}(0, 10^{-2})$, and those of the backscatter link g_k $(1 \le k \le K)$ according the Rician distribution with Rician factor 5 [20], [43]. Unless otherwise mentioned, the false alarm probabilities $P_{\text{FA}}^{\text{CD}}$, $P_{\text{FA}}^{\text{FD}}$, and $P_{\text{FA}}^{\text{BD}}$ are set as 0.05 [45]. Since the noise is not a controllable factor, we do not consider the noise in specialized frequency bandwidth and normalize the noise power, i.e., $\omega_m(n) \sim \mathcal{CN}(0, 1)$ [15]–[17]. Moreover, the signal amplitude attenuation inside the tag α is 0.5.

The detection probabilities of the CD versus SNR for different number of optimal selected antennas M are shown in Fig. 4. The curves have been depicted for two cases of known size relationship (kSR) and unknown size relationship (ukSR) between the CSI h and μ_{κ_m}. For comparison, we also plot the theoretical detection probabilities (27) and (26), and the bounds of detection probability (18), (19), (23) and (24). The number of tag antennas and RF signals are set as $K = 6$ and $N = 300$, respectively. Fig. 4 shows that

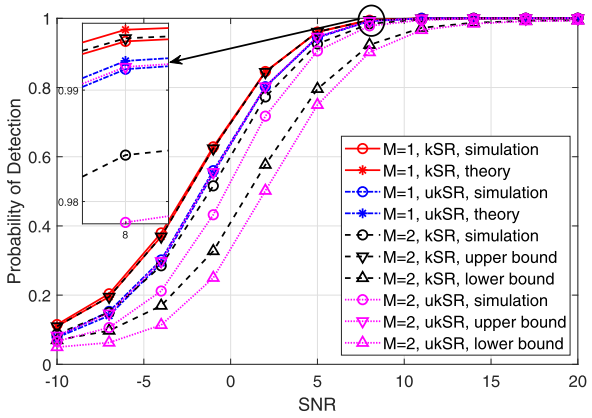

Fig. 4. CD: P_D^{CD} versus SNR for different number of backscatter antennas M.

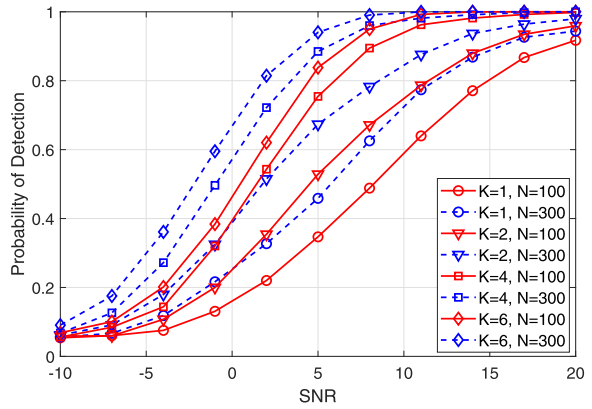

Fig. 5. CD: P_D^{CD} versus SNR for different number of candidate antennas K and RF signals N.

our theoretical conclusions match the simulation results. More importantly, selecting fewer antennas (smaller M) contributes to a better performance, which corroborates the Corollary 3. The reason is that choosing fewer backscatter antennas according to the optimal antenna selection algorithm (29) causes a bigger energy difference (28).

Fig. 5 demonstrates the impact of number of antennas K and number of RF signals N over detection probability of the CD when size relationship between the CSI h and μ_{κ_m} is unknown. We choose only one antenna according to (29) and plot the simulated detection probabilities when $K = 1, 2, 4, 6$, and $N = 100, 300$, respectively. Clearly, the detection probability increases as the value of K or N climbs up. This is because multiple antennas at the tag provide the diversity gain [29], and the larger N leads to more uncorrelated RF signals.

Fig. 6 illustrates FD detection probabilities versus SNR when two $(M = 2)$ or four $(M = 4)$ backscatter antennas are selected optimally. We also depict the cases of known CSI (denoted kCSI) μ_{κ_m} and unknown CSI (denoted ukCSI) μ_{κ_m}. The theoretical detection probabilities (51) and (52) and the derived bounds (47), (47), (49) and (50) are plotted for comparison. Interestingly, the detection probability increases as the number of selected antennas M decreases, due to the fact that

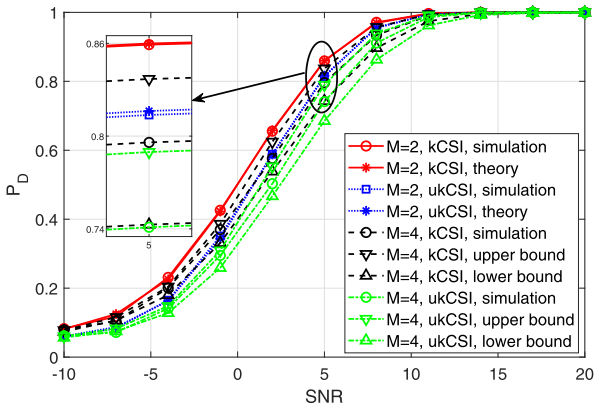

Fig. 6. FD: P_D^{FD} versus SNR for different number of backscatter antennas M.

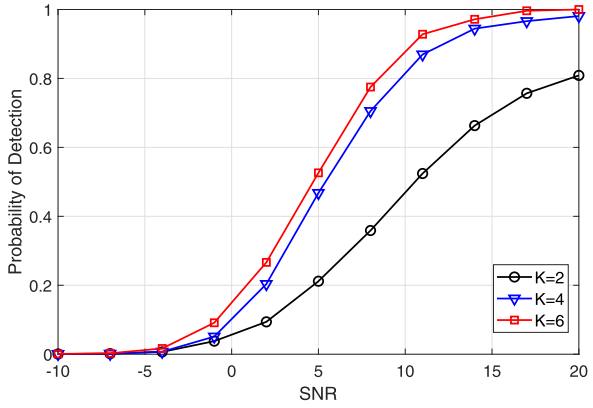

Fig. 8. BD: P_D^{BD} versus SNR for different number of candidate antennas K.

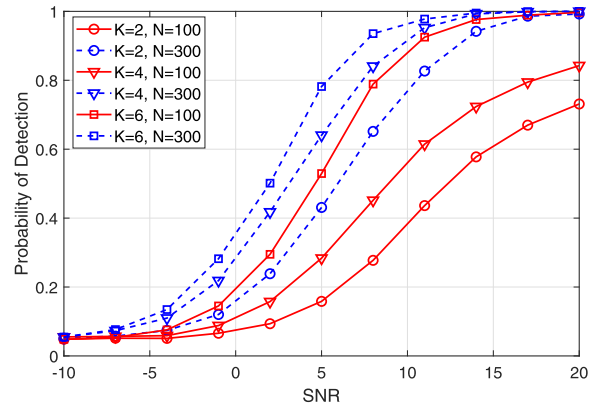

Fig. 7. FD: P_D^{FD} versus SNR for different number of candidate antennas K and RF signals N.

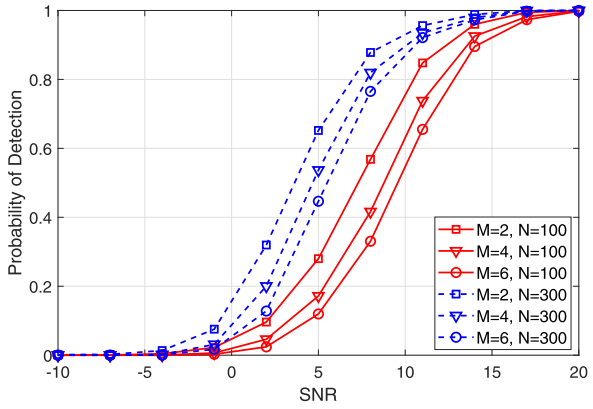

Fig. 9. BD: P_D^{BD} versus SNR for different number of backscatter antennas M and RF signals N.

less backscatter antennas according to Algorithm 1 results in larger energy difference (53), which corroborates Corollary 6.

Fig. 7 depicts the detection probability of the FD against SNR without the CSI μ_{κ_m} when the number of antennas is $K = 2, 4, 6$ and the number of RF signals is $N = 100, 300$, respectively. We select two antennas ($M = 2$) and adopt Algorithm 1 in Section IV-C to choose the antennas corresponding to the maximum and the minimum channel modulus. We see that the detection probabilities trend upward with more antennas and more RF signals, which contribute to more uncorrelated RF signals.

In Fig. 8, detection probabilities of the BD versus SNR are plotted for different numbers of the selected antennas M. Other parameters remain the same as those in Fig. 4. We observe that a smaller value of M, i.e., choosing fewer backscattering antennas, leads to larger energy difference (53) and thus improves the detection performance.

Fig. 9 shows how the detection probability of the BD varies versus SNR for various combinations of the number of antennas K and the number of RF signals N. As can be observed, for certain SNRs, the detection performance improves significantly with the availability of more signals; moreover, the performance for $N = 300$ is always better than that of $N = 100$. Similarly, more antennas improves the detection performance.

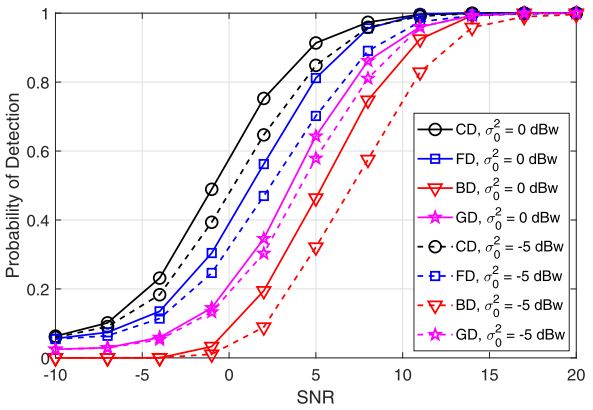

Fig. 10. Performance comparison: P_D versus SNR.

Fig. 10 compares the three detectors for noise variances $\sigma_0^2 = 0$ dBw and $\sigma_0^2 = -5$ dBw when both the CSI μ_{κ_m} and the size relationship between h and μ_{κ_m} are unknown. The number of antennas K is set to six, and two backscatter antennas ($M = 2$) are selected. We observe that although the CD outperforms the other two detectors, it requires perfect knowledge of the RF signal power, the noise variance and the CSI h at the reader. However, the FD and BD perform

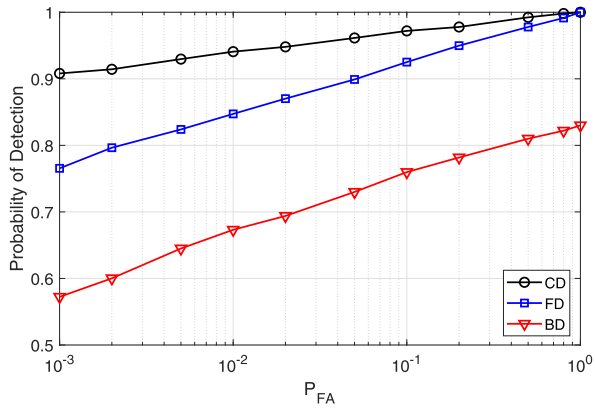

Fig. 11. Performance comparison: P_D versus $P_{\rm FA}$.

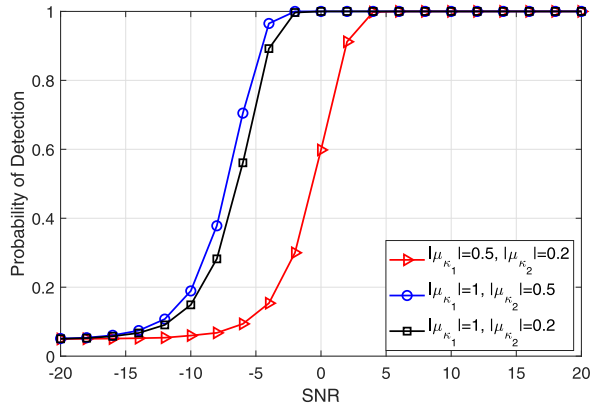

Fig. 12. CD: $P_D^{\rm CD}$ under different antenna sets.

close to that of CD, especially at high SNR. This trend is also clear from Fig. 11, where the detection performance of the three proposed detectors in terms of the false alarm probability $P_{\rm FA}$ for an 8 dB SNR has been illustrated. For comparison, we also depict the detection performance of the blind GLRT detector (GD) [34] in Fig. 10. We observe that the proposed CD and FD outperform the blind GD. In addition, lower noise variance leads to better detection performance of the proposed three detectors.

Next, we examine the optimal antenna selection schemes for the CD (Section III-C). In this experiment, the number of RF signals is set as $N = 300$ and the number of selected antennas is $M = 2$. The candidate antenna set includes $K = 3$ antennas, whose corresponding channel modulus are $|\mu_1| = 1$, $|\mu_2| = 0.5, |\mu_3| = 0.2$, respectively. Three backscatter antenna sets $\mathcal{B} = \{\kappa_1, \kappa_2\}$ are investigated: $\{1, 2\}$, $\{1, 3\}$ and $\{2, 3\}$, and their corresponding detection probabilities are plotted (Fig. 12). We see that the optimal backscatter antenna set maximizing the detection probability is composed of the antennas with two largest channel modulus, i.e., $\mathcal{B}_{opt} = \{1, 2\}$, which corroborates our suggested optimal antenna selection scheme (29).

Finally, the detection performance of the optimal antenna selection schemes proposed in Algorithm 1 for the FD and the BD is illustrated in Fig. 13. The number of RF signals is $N = 300$ and the number of selected antennas is $M = 3$.

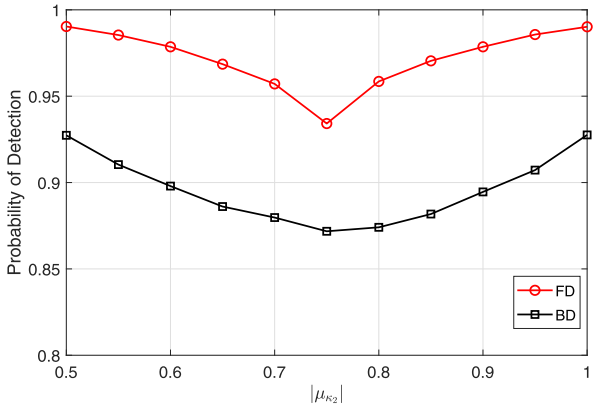

Fig. 13. FD and BD: $P_D^{\rm FD}$ and $P_D^{\rm BD}$ versus $|\mu_{\kappa_2}|$.

Denote the backscatter antenna set as $\{\kappa_1, \kappa_2, \kappa_3\}$ and the corresponding channel modulus as $\{|\mu_{\kappa_1}|, |\mu_{\kappa_2}|, |\mu_{\kappa_3}|\}$. We set $|\mu_{\kappa_1}| = 1.1$, $|\mu_{\kappa_3}| = 0.4$ and then plot the detection probabilities when the values of $|\mu_{\kappa_2}|$ range between 0.5 and 1. Fig. 13 shows that the maximum detection probability of the FD and the BD are both achieved when $|\mu_{\kappa_2}| = 0.5$ or $|\mu_{\kappa_2}| = 1$, which agrees with our theoretical analysis in Section IV-C and Section V-B.

VII. Conclusion

We investigated the signal detection problem for ambient backscatter systems with multiple-antenna tags. Specifically, a chi-squared detector was proposed to recover the tag signals without the knowledge of multiple channel parameters. Further, two blind detectors were derived to avoid all CSI and the knowledge of the RF signal power and noise variance. The detection probability bounds for the chi-squared and the F-test detectors were derived. We also developed optimal antenna selection schemes to maximize the detection performance. We found that multiple-antenna tags could achieve large gains over single-antenna tags and that the chi-squared detector outperforms the other two blind detectors at low SNR. But their performances tend to converge in the high SNR regime. We hasten to add that multi-antenna tags open up a myriad of future research directions towards more data-intensive and more energy-efficiency IoT applications. These include the utilization of more sophisticated modulation of RF signals (e.g., space time coding), the integration of wireless power transfer technologies, and the exploration of tag selection scheme based on multi-antenna techniques.

Appendix A
Proof of Theorem 1

Clearly, the distribution of the decision statistic $T_{\rm CD}$ under $\mathcal{H}_0$ is necessary for the computation of the detection probability, but is hard to derive. Instead, we define another statistic under $\mathcal{H}_1$

$$T_{\rm CD1} = \sum_{m=1}^{M} \frac{2\|\mathbf{y}_m\|_2^2}{|\mu_{\kappa_m}|^2 P_s + \sigma_0^2} \sim \chi_{2N}^2. \tag{64}$$

Under the assumption in (17), the statistic under $\mathcal{H}_1$ given in (64) is bounded as

$$\eta_{lb}^{\mathrm{CD}} T_{\mathrm{CD}} < T_{\mathrm{CD1}} < \eta_{ub}^{\mathrm{CD}} T_{\mathrm{CD}} \tag{65}$$

Thus the lower bound of the detection probability $P_{D,lb}^{\mathrm{CD}}$ can be obtained by

$$\begin{aligned} P_D^{\mathrm{CD}} &= \Pr\{T_{\mathrm{CD}} < \gamma_l^{\mathrm{CD}}; \mathcal{H}_1\} + \Pr\{T_{\mathrm{CD}} > \gamma_r^{\mathrm{CD}}; \mathcal{H}_1\} \\ &> \Pr\Big\{\frac{T_{\mathrm{CD1}}}{\eta_{lb}^{\mathrm{CD}}} < \gamma_l^{\mathrm{CD}}; \mathcal{H}_1\Big\} + \Pr\Big\{\frac{T_{\mathrm{CD1}}}{\eta_{ub}^{\mathrm{CD}}} > \gamma_r^{\mathrm{CD}}; \mathcal{H}_1\Big\}, \end{aligned} \tag{66}$$

and similarly, the upper bound $P_{D,ub}^{\mathrm{CD}}$ can be calculated as

$$P_D^{\mathrm{CD}} < \Pr\Big\{\frac{T_{\mathrm{CD1}}}{\eta_{ub}^{\mathrm{CD}}} < \gamma_l^{\mathrm{CD}}; \mathcal{H}_1\Big\} + \Pr\Big\{\frac{T_{\mathrm{CD1}}}{\eta_{lb}^{\mathrm{CD}}} > \gamma_r^{\mathrm{CD}}; \mathcal{H}_1\Big\}. \tag{67}$$

Since the decision statistic T_{CD1} (64) is a chi-squared RV with degrees of freedom $2N$ under $\mathcal{H}_1$, the lower bound (18) and upper bound (19) can be directly obtained from (66) and (67), respectively.

Appendix B
Proof of Theorem 2

In the case of $|h| < |\mu_{\kappa_M}|$, the statistic $\dfrac{2\|\mathbf{y}\|_2^2}{N(|h|^2P_s+\sigma_0^2)}$ approximates 1 under $\mathcal{H}_0$ while is hopefully larger than 1 under $\mathcal{H}_1$. Thus, the detection rule (11) can be reformulated as one-sided test (20). The threshold γ_1^{CD} given in (21) is obtained from the false alarm probability

$$P_{\mathrm{FA}}^{\mathrm{CD}} = \Pr\{T_{\mathrm{CD}} > \gamma_1^{\mathrm{CD}}; \mathcal{H}_0\} = Q_{\chi_{2N}^2}\left(\frac{2\gamma_1^{\mathrm{CD}}}{|h|^2P_s+\sigma_0^2}\right). \tag{68}$$

Then from (65), we can obtain the bounds of detection probability $P_D^{\mathrm{CD}} = \Pr\{T_{\mathrm{CD}} > \gamma_1^{\mathrm{CD}}; \mathcal{H}_1\}$ through

$$\Pr\Big\{\frac{T_{\mathrm{CD1}}}{\eta_{lb}^{\mathrm{CD}}} > \gamma_1^{\mathrm{CD}}; \mathcal{H}_1\Big\} < P_D^{\mathrm{CD}} < \Pr\Big\{\frac{T_{\mathrm{CD1}}}{\eta_{ub}^{\mathrm{CD}}} > \gamma_1^{\mathrm{CD}}; \mathcal{H}_1\Big\}, \tag{69}$$

which lead to the lower bound (23) and the upper bound (24) in the case of $|h| < |\mu_{\kappa_M}|$ through straightforward computation since T_{CD1} has chi-squared distribution.

The proof for the case of $|h| > |\mu_{\kappa_1}|$ is similar as the case of $|h| < |\mu_{\kappa_M}|$ and the proof for the case of $|\mu_{\kappa_M}| < |h| < |\mu_{\kappa_1}|$ is the same as the proof of Theorem 1.

Appendix C
Proof of Proposition 1

The energy of the received signals $\mathbf{y}$ (6) under $\mathcal{H}_0$ and $\mathcal{H}_1$ can be calculated as

$$\begin{aligned} \mathbb{E}_{\mathbf{x},\omega}\{\|\mathbf{y}\|_2^2; \mathcal{H}_0\} &= |h|^2\mathbb{E}_{\mathbf{x}}\{\mathbf{x}^H\mathbf{x}\} + N\sigma_0^2 \\ &= N(|h|^2P_s+\sigma_0^2), \end{aligned} \tag{70}$$

and

$$\begin{aligned} \mathbb{E}_{\mathbf{x},\omega}\{\|\mathbf{y}\|_2^2; \mathcal{H}_1\} &= \mathbb{E}_{\mathbf{x}}\{\mathbf{x}^H\mathbf{F}^H\mathbf{F}\mathbf{x}\} + N\sigma_0^2 \\ &= \sum_{m=1}^{M}\left(N_m|\mu_{\kappa_m}|^2P_s+\sigma_0^2\right), \end{aligned} \tag{71}$$

where $\mathbb{E}_{\mathbf{x}}\{\mathbf{x}^H\mathbf{F}^H\mathbf{F}\mathbf{x}\} = P_s\mathrm{trace}(\mathbf{F}\mathbf{F}^H)$. The energy difference (28) can be further derived as

$$\delta_E = \Big|\sum_{m=1}^{M} N_m|\mu_{\kappa_m}|^2 - N|h|^2\Big|P_s. \tag{72}$$

Our aim is to maximize the energy difference (28) of the received signals between $\mathcal{H}_0$ and $\mathcal{H}_1$. Given the value of M, when $|\mu_K| \geq |h|$, the energy difference (72) can be simplified as $\sum_{m=1}^{M} N_m|\mu_{\kappa_m}|^2P_s - N|h|^2P_s$. So we select the antennas with the first M largest channel gain, i.e., $\mathcal{B}_1 = \{1, 2, \ldots, M\}$.

Similarly, in the case of $|h| > |\mu_1|$, the energy difference (72) is reduced to $N|h|^2P_s - \sum_{m=1}^{M} N_m|\mu_{\kappa_m}|^2P_s$ and the optimal backscatter antenna set contains the antennas with the last M smallest channel gain, i.e., $\mathcal{B}_2 = \{K-M+1, K-M+2, \ldots, K\}$.

Finally, when $|\mu_K| < |h| < |\mu_1|$, the energy difference (28) will reach the maximum value in either $\mathcal{B}_1$ or $\mathcal{B}_2$ case. Therefore, from the two cases, we choose the optimal one that can maximize the energy difference (72).

Appendix D
Proof of Corollary 3

When $|\mu_K| > |h|$, the energy difference δ_E (72) is bounded as

$$\begin{aligned} \delta_E &= \sum_{m=1}^{M} N_m|\mu_{\kappa_m}|^2P_s - N|h|^2P_s \\ &\leq N|\mu_{\kappa_1}|^2P_s - N|h|^2P_s \leq N(|\mu_1|^2 - |h|^2)P_s. \end{aligned} \tag{73}$$

So the maximal energy difference is obtained when we choose only one antenna with the largest channel modulus $|\mu_1|$.

Similarly when $|h| > |\mu_1|$, we have

$$\begin{aligned} \delta_E &= N|h|^2P_s - \sum_{m=1}^{M} N_m|\mu_{\kappa_m}|^2P_s \\ &\leq N|h|^2P_s - N|\mu_{\kappa_M}|^2P_s \leq N(|h|^2 - |\mu_K|^2)P_s. \end{aligned} \tag{74}$$

As a result, to maximize the energy difference, we design $M = 1$ and choose the antenna with the smallest channel modulus $|\mu_K|$.

Appendix E
Proof of Theorem 3

From (17), it can be readily checked that

$$\frac{\|\mathbf{y}_u\|_2^2}{|\mu_{\kappa_1}|^2P_s+\sigma_0^2} < \mathbf{y}_u^H\mathbf{C}_{u1}^{-1}\mathbf{y}_u < \frac{\|\mathbf{y}_u\|_2^2}{|\mu_{\kappa_{\tilde{m}}}|^2P_s+\sigma_0^2}, \tag{75}$$

and

$$\frac{\|\mathbf{y}_d\|_2^2}{|\mu_{\kappa_{\tilde{m}+1}}|^2P_s+\sigma_0^2} < \mathbf{y}_d^H\mathbf{C}_{d1}^{-1}\mathbf{y}_d < \frac{\|\mathbf{y}_d\|_2^2}{|\mu_{\kappa_M}|^2P_s+\sigma_0^2}. \tag{76}$$

Then the statistic $T_{\text{FD1}} = \dfrac{N_d \mathbf{y}_u^H \mathbf{C}_{u1}^{-1} \mathbf{y}_u}{N_u \mathbf{y}_d^H \mathbf{C}_{d1}^{-1} \mathbf{y}_d}$ (43) is bounded as

$$\eta_{lb}^{\text{FD}} T_{\text{FD}} < T_{\text{FD1}} < \eta_{ub}^{\text{FD}} T_{\text{FD}}. \tag{77}$$

The lower bound $P_{D,lb}^{\text{FD}}$ of the detection probability is obtained as

$$\begin{aligned} P_D^{\text{FD}} &= \Pr\{T_{\text{FD}} < \gamma_l^{\text{FD}}; \mathcal{H}_1\} + \Pr\{T_{\text{FD}} > \gamma_r^{\text{FD}}; \mathcal{H}_1\} \\ &> \Pr\Big\{\frac{T_{\text{FD1}}}{\eta_{lb}^{\text{FD}}} < \gamma_l^{\text{FD}}; \mathcal{H}_1\Big\} + \Pr\Big\{\frac{T_{\text{FD1}}}{\eta_{ub}^{\text{FD}}} > \gamma_r^{\text{FD}}; \mathcal{H}_1\Big\}, \end{aligned} \tag{78}$$

and the upper bound $P_{D,ub}^{\text{FD}}$ is given by

$$P_D^{\text{FD}} < \Pr\Big\{\frac{T_{\text{FD1}}}{\eta_{ub}^{\text{FD}}} < \gamma_l^{\text{FD}}; \mathcal{H}_1\Big\} + \Pr\Big\{\frac{T_{\text{FD1}}}{\eta_{lb}^{\text{FD}}} > \gamma_r^{\text{FD}}; \mathcal{H}_1\Big\}. \tag{79}$$

Since T_{FD1} (43) is an F RV with degrees of freedom $2N_u$ and $2N_d$ under $\mathcal{H}_1$, the lower bound (47) and upper bound (47) are obtained after some straightforward computation.

Appendix F
Proof of Theorem 4

Given the CSI μ_{κ_m}, we reorganize the received signals $\mathbf{y}$ into two parts, $\mathbf{y}_u$ and $\mathbf{y}_d$, which are from the selected antennas with first largest $\tilde{m}$ channel modulus and last smallest $M-\tilde{m}$ channel modulus, separately. Then the sample variance of $\mathbf{y}_u$ is always larger than the sample variance $\mathbf{y}_d$. As a result, the decision rule (39) is translated into one-sided test (47).

Accordingly, the false alarm probability can be given by

$$\begin{aligned} P_{\text{FA}}^{\text{FD}} &= \Pr\{T_{\text{FD}} > \gamma_{\text{FD}}; \mathcal{H}_0\} = \Pr\Big\{T_{\text{FD0}} > \frac{N_d}{N_u}\gamma_{\text{FD}}; \mathcal{H}_0\Big\} \\ &= Q_{F(2N_u, 2N_d)}\left(\frac{N_d}{N_u}\gamma_{\text{FD}}\right), \end{aligned} \tag{80}$$

which can directly produce the detection threshold (48).

From (77), the bounds of the detection probability $P_D^{\text{FD}} = \Pr\{T_{\text{FD}} > \gamma_{\text{FD}}; \mathcal{H}_1\}$ can be derived as

$$\Pr\Big\{\frac{T_{\text{FD1}}}{\eta_{ub}^{\text{FD}}} > \gamma_{\text{FD}}; \mathcal{H}_1\Big\} < P_D^{\text{FD}} < \Pr\Big\{\frac{T_{\text{FD1}}}{\eta_{lb}^{\text{FD}}} > \gamma_{\text{FD}}; \mathcal{H}_1\Big\}. \tag{81}$$

Similar as the proof of Theorem 3, the lower bound (49) and upper bound (50) are obtained after some straightforward computation.

Appendix G
Proof of Corollary 6

The average power of the first part of received signals $\mathbf{y}_u$ (54) is bounded as

$$\begin{aligned} \mathbb{E}_{\mathbf{x}_u, \omega_u}\{\|\mathbf{y}_u\|_2^2\} &= \sum_{m=1}^{\tilde{m}} N_m \left(|\mu_{\kappa_m}|^2 P_s + \sigma_0^2\right) \\ &\le \sum_{m=1}^{\tilde{m}} N_m \left(|\mu_{\kappa_1}|^2 P_s + \sigma_0^2\right) \\ &\le \sum_{m=1}^{\tilde{m}} N_m \left(|\mu_1|^2 P_s + \sigma_0^2\right). \end{aligned} \tag{82}$$

Similarly, from (55) we obtain

$$\begin{aligned} \mathbb{E}_{\mathbf{x}_d, \omega_d}\{\|\mathbf{y}_d\|_2^2\} &= \sum_{m=\tilde{m}+1}^{M} N_m \left(|\mu_{\kappa_m}|^2 P_s + \sigma_0^2\right) \\ &\ge \sum_{m=\tilde{m}+1}^{M} N_m \left(|\mu_{\kappa_M}|^2 P_s + \sigma_0^2\right) \\ &\ge \sum_{m=\tilde{m}+1}^{M} N_m \left(|\mu_K|^2 P_s + \sigma_0^2\right). \end{aligned} \tag{83}$$

Thus, to maximize the energy difference between $\mathbf{y}_u$ and $\mathbf{y}_d$, two antennas are to be selected, i.e., $M = 2$, and the optimal backscatter antenna set is $\mathcal{B}_{opt} = \{1, K\}$.

References

[1] A. Al-Fuqaha, M. Guizani, M. Mohammadi, M. Aledhari, and M. Ayyash, "Internet of Things: A survey on enabling technologies, protocols, and applications," *IEEE Commun. Surveys Tuts.*, vol. 17, no. 4, pp. 2347–2376, 2015.

[2] G. Park, T. Rosing, M. D. Todd, C. R. Farrar, and W. Hodgkiss, "Energy harvesting for structural health monitoring sensor networks," *J. Infrastruct. Syst.*, vol. 14, no. 1, pp. 64–79, Mar. 2008.

[3] V. Liu, A. Parks, V. Talla, S. Gollakota, D. Wetherall, and J. Smith, "Ambient backscatter: Wireless communication out of thin air," in *Proc. ACM SIGCOMM*, Hong Kong, Aug. 2013, pp. 39–50.

[4] H. Stockman, "Communication by means of reflected power," *Proc. IRE*, vol. 36, no. 10, pp. 1196–1204, Oct. 1948.

[5] C. Boyer and S. Roy, "—Invited paper—Backscatter communication and RFID: Coding, energy, and MIMO analysis," *IEEE Trans. Commun.*, vol. 62, no. 3, pp. 770–785, Mar. 2014.

[6] D. Dobkin, *The RF in RFID: UHF RFID in Practice*. Newnes, NSW, Australia: Elsevier, 2008.

[7] N. Van Huynh, D. T. Hoang, X. Lu, D. Niyato, P. Wang, and D. I. Kim, "Ambient backscatter communications: A contemporary survey," *IEEE Commun. Surveys Tuts.*, vol. 20, no. 4, pp. 2889–2922, 4th Quart., 2018.

[8] B. Kellogg, A. Parks, S. Gollakota, J. R. Smith, and D. Wetherall, "Wi-Fi backscatter: Internet connectivity for RF-powered devices," in *Proc. ACM Conf. SIGCOMM (SIGCOMM)*, Chicago, IL, USA, Aug. 2014, pp. 607–618.

[9] A. N. Parks, A. Liu, S. Gollakota, and J. R. Smith, "Turbocharging ambient backscatter communication," *SIGCOMM Comput. Commun. Rev.*, vol. 44, no. 4, pp. 619–630, Aug. 2014.

[10] B. Kellogg, V. Talla, S. Gollakota, and J. Smith, "Passive Wi-Fi: Bringing low power to Wi-Fi transmissions," in *Proc. NSDI*, Santa Clara, CA, USA, Mar. 2016, pp. 151–164.

[11] S. Ma, G. Wang, R. Fan, and C. Tellambura, "Blind channel estimation for ambient backscatter communication systems," *IEEE Commun. Lett.*, vol. 22, no. 6, pp. 1296–1299, Jun. 2018.

[12] W. Zhao, G. Wang, S. Atapattu, R. He, and Y.-C. Liang, "Channel estimation for ambient backscatter communication systems with massive-antenna reader," *IEEE Trans. Veh. Technol.*, vol. 68, no. 8, pp. 8254–8258, Aug. 2019.

[13] D. Mishra and E. G. Larsson, "Optimal channel estimation for reciprocity-based backscattering with a full-duplex MIMO reader," *IEEE Trans. Signal Process.*, vol. 67, no. 6, pp. 1662–1677, Mar. 2019.

[14] G. Wang, F. Gao, R. Fan, and C. Tellambura, "Ambient backscatter communication systems: Detection and performance analysis," *IEEE Trans. Commun.*, vol. 64, no. 11, pp. 4836–4846, Nov. 2016.

[15] J. Qian, F. Gao, G. Wang, S. Jin, and H. Zhu, "Noncoherent detections for ambient backscatter system," *IEEE Trans. Wireless Commun.*, vol. 16, no. 3, pp. 1412–1422, Mar. 2017.

[16] J. Qian, F. Gao, G. Wang, S. Jin, and H. Zhu, "Semi-coherent detection and performance analysis for ambient backscatter system," *IEEE Trans. Commun.*, vol. 65, no. 12, pp. 5266–5279, Dec. 2017.

[17] H. Guo, Q. Zhang, S. Xiao, and Y.-C. Liang, "Exploiting multiple antennas for cognitive ambient backscatter communication," *IEEE Internet Things J.*, vol. 6, no. 1, pp. 765–775, Feb. 2019.

[18] S. Ma, G. Wang, Y. Wang, and Z. Zhao, "Signal ratio detection and approximate performance analysis for ambient backscatter communication systems with multiple receiving antennas," *Mobile Netw. Appl.*, vol. 23, no. 6, pp. 1478–1486, Dec. 2018.
[19] Q. Zhang, H. Guo, Y.-C. Liang, and X. Yuan, "Constellation learning-based signal detection for ambient backscatter communication systems," *IEEE J. Sel. Areas Commun.*, vol. 37, no. 2, pp. 452–463, Feb. 2019.
[20] G. Yang, Q. Zhang, and Y.-C. Liang, "Cooperative ambient backscatter communications for green Internet-of-Things," *IEEE Internet Things J.*, vol. 5, no. 2, pp. 1116–1130, Apr. 2018.
[21] J. Wang and M. Bolic, "Exploiting dual-antenna diversity for phase cancellation in augmented RFID system," in *Proc. Int. Conf. Smart Commun. Netw. Technol. (SaCoNeT)*, Vilanova i la Geltrú, Spain, Jun. 2014, pp. 1–6.
[22] Q. Tao, C. Zhong, H. Lin, and Z. Zhang, "Symbol detection of ambient backscatter systems with manchester coding," *IEEE Trans. Wireless Commun.*, vol. 17, no. 6, pp. 4028–4038, Jun. 2018.
[23] X. Zhou, G. Wang, Y. Wang, and J. Cheng, "An approximate BER analysis for ambient backscatter communication systems with tag selection," *IEEE Access*, vol. 5, pp. 22552–22558, 2017.
[24] D. Li, W. Peng, and F. Hu, "Capacity of backscatter communication systems with tag selection," *IEEE Trans. Veh. Technol.*, vol. 68, no. 10, pp. 10311–10314, Oct. 2019.
[25] C. Psomas and I. Krikidis, "Backscatter communications for wireless powered sensor networks with collision resolution," *IEEE Wireless Commun. Lett.*, vol. 6, no. 5, pp. 650–653, Oct. 2017.
[26] W. Zhao, G. Wang, S. Atapattu, C. Tellambura, and H. Guan, "Outage analysis of ambient backscatter communication systems," *IEEE Commun. Lett.*, vol. 22, no. 8, pp. 1736–1739, Aug. 2018.
[27] G. Yang, Y.-C. Liang, R. Zhang, and Y. Pei, "Modulation in the air: Backscatter communication over ambient OFDM carrier," *IEEE Trans. Commun.*, vol. 66, no. 3, pp. 1219–1233, Mar. 2018.
[28] D. Darsena, G. Gelli, and F. Verde, "Modeling and performance analysis of wireless networks with ambient backscatter devices," *IEEE Trans. Commun.*, vol. 65, no. 4, pp. 1797–1814, Apr. 2017.
[29] J. D. Griffin and G. D. Durgin, "Gains for RF tags using multiple antennas," *IEEE Trans. Antennas Propag.*, vol. 56, no. 2, pp. 563–570, Feb. 2008.
[30] C. Boyer and S. Roy, "Space time coding for backscatter RFID," *IEEE Trans. Wireless Commun.*, vol. 12, no. 5, pp. 2272–2280, May 2013.
[31] C. He and Z. J. Wang, "Closed-form BER analysis of non-coherent FSK in MISO double Rayleigh fading/RFID channel," *IEEE Commun. Lett.*, vol. 15, no. 8, pp. 848–850, Aug. 2011.
[32] S. Kay, *Fundamentals of Statistical Signal Processing: Detection Theory*, vol. 2. Upper Saddle River, NJ, USA: Prentice-Hall, 1998.
[33] C. Chen, G. Wang, F. Gao, Y. C. Eldar, and H. Guan, "blind detection for ambient backscatter communication system with multiple-antenna tags," in *Proc. IEEE Global Commun. Conf. (GLOBECOM)*, Abu Dhabi, United Arab Emirates, Dec. 2018, pp. 1–6.
[34] C. Chen, G. Wang, P. D. Diamantoulakis, R. He, G. K. Karagiannidis, and C. Tellambura, "Signal detection and optimal antenna selection for ambient backscatter communications with multi-antenna tags," *IEEE Trans. Commun.*, vol. 68, no. 1, pp. 466–479, Jan. 2020, doi: 10.1109/tcomm.2019.2946799.
[35] R. Zhang, T. Lim, Y.-C. Liang, and Y. Zeng, "Multi-antenna based spectrum sensing for cognitive radios: A GLRT approach," *IEEE Trans. Commun.*, vol. 58, no. 1, pp. 84–88, Jan. 2010.
[36] C.-H. Kang, W.-S. Lee, Y.-H. You, and H.-K. Song, "Signal detection scheme in ambient backscatter system with multiple antennas," *IEEE Access*, vol. 5, pp. 14543–14547, 2017.
[37] C. Chen, G. Wang, R. He, F. Gao, and Z. Li, "Semi-blind detection of ambient backscatter signals from multiple-antenna tags," in *Proc. 24th Asia–Pacific Conf. Commun. (APCC)*, Ningbo, China, Nov. 2018, pp. 570–575.
[38] G. Snedecor and W. Cochran, *Statistical methods*, 8th ed. Ames, IA, USA: Iowa State Univ. Press, 1989.
[39] D. Gesbert, H. Bolcskei, D. Gore, and A. Paulraj, "MIMO wireless channels: Capacity and performance prediction," in *Proc. IEEE. Global Telecommun. Conf. (Globecom)*, San Francisco, CA, USA, vol. 2, Nov. 2002, pp. 1083–1088.
[40] J. R. Smith, A. P. Sample, P. S. Powledge, S. Roy, and A. Mamishev, "A wirelessly-powered platform for sensing and computation," in *Proc. Ubicomp*, Heidelberg, Germany, 2006, pp. 495–506.
[41] X. Lu, P. Wang, D. Niyato, D. I. Kim, and Z. Han, "Wireless networks with RF energy harvesting: A contemporary survey," *IEEE Commun. Surveys Tuts.*, vol. 17, no. 2, pp. 757–789, 2nd Quart., 2015.
[42] R. Zhang and C. K. Ho, "MIMO broadcasting for simultaneous wireless information and power transfer," *IEEE Trans. Wireless Commun.*, vol. 12, no. 5, pp. 1989–2001, May 2013.
[43] J. Qian, A. N. Parks, J. R. Smith, F. Gao, and S. Jin, "IoT communications with M-PSK modulated ambient backscatter: Algorithm, analysis, and implementation," *IEEE Internet Things J.*, vol. 6, no. 1, pp. 844–855, Feb. 2019.
[44] N. Johnson, S. Kotz, and N. Balakrishnan, *Continuous Univariate Distributions* (Wiley Series in Probability and Mathematical Statistics: Applied Probability and Statistics), vol. 2. New York, NY, USA: Wiley, 1995.
[45] A. Razavi, M. Valkama, and D. Cabric, "Compressive detection of random subspace signals," *IEEE Trans. Signal Process.*, vol. 64, no. 16, pp. 4166–4179, Aug. 2016.
[46] P. R. Killeen, "An alternative to null-hypothesis significance tests," *Psychol. Sci.*, vol. 16, no. 5, pp. 345–353, May 2005.

Chen Chen received the B.Eng. degree in Internet of Things from Beijing Jiaotong University, Beijing, China, in 2016, where she is currently pursuing the Ph.D. degree with the School of Computer and Information Technology. Her research interests include signal processing in backscatter communication and wireless sensing.

Gongpu Wang (Member, IEEE) received the B.Eng. degree in communication engineering from Anhui University, Hefei, Anhui, China, in 2001, the M.Sc. degree from the Beijing University of Posts and Telecommunications, Beijing, China, in 2004, and the Ph.D. degree from University of Alberta, Edmonton, Canada, in 2011. From 2004 to 2007, he was an Assistant Professor with the School of Network Education, Beijing University of Posts and Telecommunications. He is currently a Full Professor with the School of Computer and Information Technology, Beijing Jiaotong University, China. His research interests include wireless communication, signal processing, artificial intelligence, and the Internet of Things.

Hao Guan received the M.S. and Ph.D. degrees in electrical engineering from Northern Jiaotong University, in 1996 and 1999, respectively. She started her career in industrial telecoms since 1999. She is responsible for 5G SEP technical analysis in Nokia Beijing. Before that, she had worked in radio research for Nokia Radio Research Lab for about 18 years. Her focus area is 5G Radio, 3GPP/LTE radio performance, network evolution, and interference management.

Ying-Chang Liang (Fellow, IEEE) was a Professor with The University of Sydney, Australia, a Principal Scientist and a Technical Advisor with the Institute for Infocomm Research, Singapore, and a Visiting Scholar with Stanford University, USA. He is currently a Professor with the University of Electronic Science and Technology of China, China, where he leads the Center for Intelligent Networking and Communications and serves as the Deputy Director of the Artificial Intelligence Research Institute. His research interests include wireless networking and communications, cognitive radio, symbiotic networks, dynamic spectrum access, the Internet-of-Things, artificial intelligence, and machine learning techniques.

He has been recognized by Thomson Reuters (now Clarivate Analytics) as a Highly Cited Researcher since 2014. He received the Prestigious Engineering Achievement Award from The Institution of Engineers, Singapore, in 2007, the Outstanding Contribution Appreciation Award from the IEEE Standards Association in 2011, and the Recognition Award from the IEEE Communications Society Technical Committee on Cognitive Networks, in 2018. He was a recipient of numerous paper awards, including the IEEE Jack Neubauer Memorial Award in 2014, and the IEEE Communications Society APB Outstanding Paper Award in 2012. He is a Foreign Member of Academia Europaea. He was a Distinguished Lecturer of the IEEE Communications Society and the IEEE Vehicular Technology Society. He was the Chair of the IEEE Communications Society Technical Committee on Cognitive Networks, and served as the TPC Chair and the Executive Co-Chair of the IEEE Globecom'17. He is also the Founding Editor-in-Chief of the IEEE JOURNAL ON SELECTED AREAS IN COMMUNICATIONS: COGNITIVE RADIO Series, and the Key Founder and the Editor-in-Chief of the IEEE TRANSACTIONS ON COGNITIVE COMMUNICATIONS AND NETWORKING. He is also serving as an Associate Editor-in-Chief for *China Communications*. He served as a Guest/Associate Editor for the IEEE TRANSACTIONS ON WIRELESS COMMUNICATIONS, the IEEE JOURNAL OF SELECTED AREAS IN COMMUNICATIONS, the *IEEE Signal Processing Magazine*, the IEEE TRANSACTIONS ON VEHICULAR TECHNOLOGY, and the IEEE TRANSACTIONS ON SIGNAL AND INFORMATION PROCESSING OVER NETWORK. He was also an Associate Editor-in-Chief of the World Scientific Journal on *Random Matrices: Theory and Applications*.

Chintha Tellambura (Fellow, IEEE) received the B.Sc. degree in electronics and telecommunications from the University of Moratuwa, Sri Lanka, the M.Sc. degree in electronics from the Kings College, University of London, and the Ph.D. degree in electrical engineering from the University of Victoria, Canada.

He was with Monash University, Australia, from 1997 to 2002. Since 2002, he has been with the Department of Electrical and Computer Engineering, University of Alberta, where he is currently a Full Professor. He has authored or coauthored over 560 journal and conference papers, with an H-Index of 74 (Google Scholar). He has supervised or co-supervised 66 M.Sc., Ph.D., and PDF trainees. His current research interests include cognitive radio, heterogeneous cellular networks, fifth-generation wireless networks, and machine learning algorithms. He was elected as a Fellow of The Canadian Academy of Engineering in 2017. He received the Best Paper Awards from the IEEE International Conference on Communications (ICC) in 2012 and 2017. He is the winner of the prestigious McCalla Professorship and the Killam Annual Professorship from the University of Alberta. He served as an Editor for the IEEE TRANSACTIONS ON COMMUNICATIONS from 1999 to 2012 and the IEEE TRANSACTIONS ON WIRELESS COMMUNICATIONS from 2001 to 2007. He was an Area Editor of Wireless Communications Systems and Theory from 2007 to 2012.